Nowcasting and very short range forecasting SAF

Use of MODIS to enhance the PGE01-02 of SAFNWC/MSG

17 December 2001

SAF/NWC/MFL/SCI/PSD/2, Issue 1, Rev. 0

Prepared by METEO-FRANCE/CMS

Table of contents

1. INTRODUCTION

Within SAFNWC, Meteo-France is responsible for the development of a software to extract cloud parameters from MSG SEVIRI images. The initial aim was to get the software ready before MSG is launched (initially planned in October 2000). Therefore, the algorithms and software have been prototyped with GOES and AVHRR imagery using radiative transfer modelisation. This approach has allowed to develop algorithms tuned to SEVIRI spectral characteristics, but "validated" only if a limited set of SEVIRI channels is used. Especially, the use of the new 8.7µm channel completely relies on simulation and the combination of channels has not be fully exploited.

MSG's launch has been delayed in 2002, thus allowing some more development efforts to improve the SEVIRI algorithms. Since 2000, measurements having spectral characteristics similar to SEVIRI are available from the MODIS radiometer (on board a polar-orbiting satellite called EOS-TERRA).

The objective of this study is to use the measurements from the MODIS radiometer (available on the WEB) to check and enhance the SEVIRI CMa (cloud mask) and CT (cloud type) algorithms. The present study includes:

- The validation of the cloud-free 8.7µm brightness temperatures' simulations used in the thresholds's computation (CMa)
- The analysis of the impact of the IR3.9 channel's filter's width on its ability to detect nighttime low clouds
- The analysis of the impact of simultaneous use of SEVIRI channels on the improvement of:
    - The detection of low clouds at nighttime (in arid areas and in warm sectors)
    - The distinction between sub-pixel low clouds and thin cirrus
    - The detection of snow
    - The identification of volcanic ash clouds and dust clouds
    - The cloud top phase

The ouput of the study is this report. The conclusions of this study will be used to improve the CMa/CT algorithms and software. Finally the improved software will be checked with MODIS imagery.

2. PRESENTATION AND USE OF MODIS

MODIS is a radiometer on board the polar-orbiting satellite EOS-TERRA. Its characteristics are summarised in the tables below (extracted from http://modarch.gsfc.gov/MODIS).

Primary use	Band	Bandwidth (micron)
Land/Cloud/Aerosols Boundaries	1	0.620 - 0.670
	2	0.841 - 0.876
Land/Cloud/Aerosols Properties	3	0.459 - 0.479
	4	0.545 – 0.565
	5	1.23 – 1.25
	6	1.628 – 1.652
	7	2.105 – 2.155
Ocean Color/Phytoplankton/ Biogeochemistry	8	0.405 – 0.420
	9	0.438 – 0.448
	10	0.483 – 0.493
	11	0.526 – 0.536
	12	0.546 – 0.556
	13	0.662 – 0.672
	14	0.673 – 0.683
	15	0.743 – 0.753
	16	0.862 – 0.877
Atmospheric Water Vapor	17	0.89 – 0.920
	18	0.931 – 0.941
	19	0.915 – 0.965
Surface/Cloud temperature	20	3.66 – 3.84
	21	3.929 – 3.989
	22	3.929 – 3.989
	23	4.020 – 4.080
Atmospheric temperature	24	4.443 – 4.498
	25	4.482 – 4.549
Cirrus CloudsWater vapor	26	1.36 – 1.39
	27	6.535 – 6.895
	28	7.175 – 7.475
Cloud properties	29	8.4000 – 8.700
Ozone	30	9.580 – 9.880
Surface/Cloud Temperature	31	10-780 – 11.280
	32	11.770 – 12.270
Cloud Top Temperature	33	13.185 – 13.485
	34	13.485 – 13.785
	35	13.785 – 14.085
	36	14.085 – 14-385

Orbit	705km, 10:30 a.m descending node (on Terra) or 1:30 p.m ascending node (on Aqua), sun-synchronous, near-polar, circular
Swath Dimensions	2330 km (cross track) by 10km (along track at nadir)
Quantization	12 bits
Spatial resolution	250m (band 1-2) 500m (bands 3-7) 1000m (bands 8-36)

Several WEB sites are useful:

- General information can be obtained from http://modarch.gsfc.goc/MODIS
- Information on MODIS calibration can be obtained from http://mcstweb.gsfc.nasa.gov (level 1B images from before 10th August 2000 should not be used, due to major calibration problems).
- Satellite tracks can be visualized from http: www.ssec.wisc.edu/datacenter/terra (very useful to choose imagery).
- MODIS imagery can be ordered from various WEB server. But the images are located at GSFC/NASA (MaryLand).
    - http://acdisx.gsfc.nasa.gov/data
    - http://ims.dfd.dlr.de/pub/mswelcome/index.html
    - http://redhook.gsfc.nasa.gov/~imswww/pub/welcome

In this study, we only use MODIS channels that are similar to SEVIRI channels, ie., MODIS channels 01, 02, 06, 20-23 (except 21), 27, 28, 29, 31, 32, 33-36. The following figures compare the spectral response of MSG channels (in green solid lines) and the equivalent MODIS channels (in brown dotted lines).

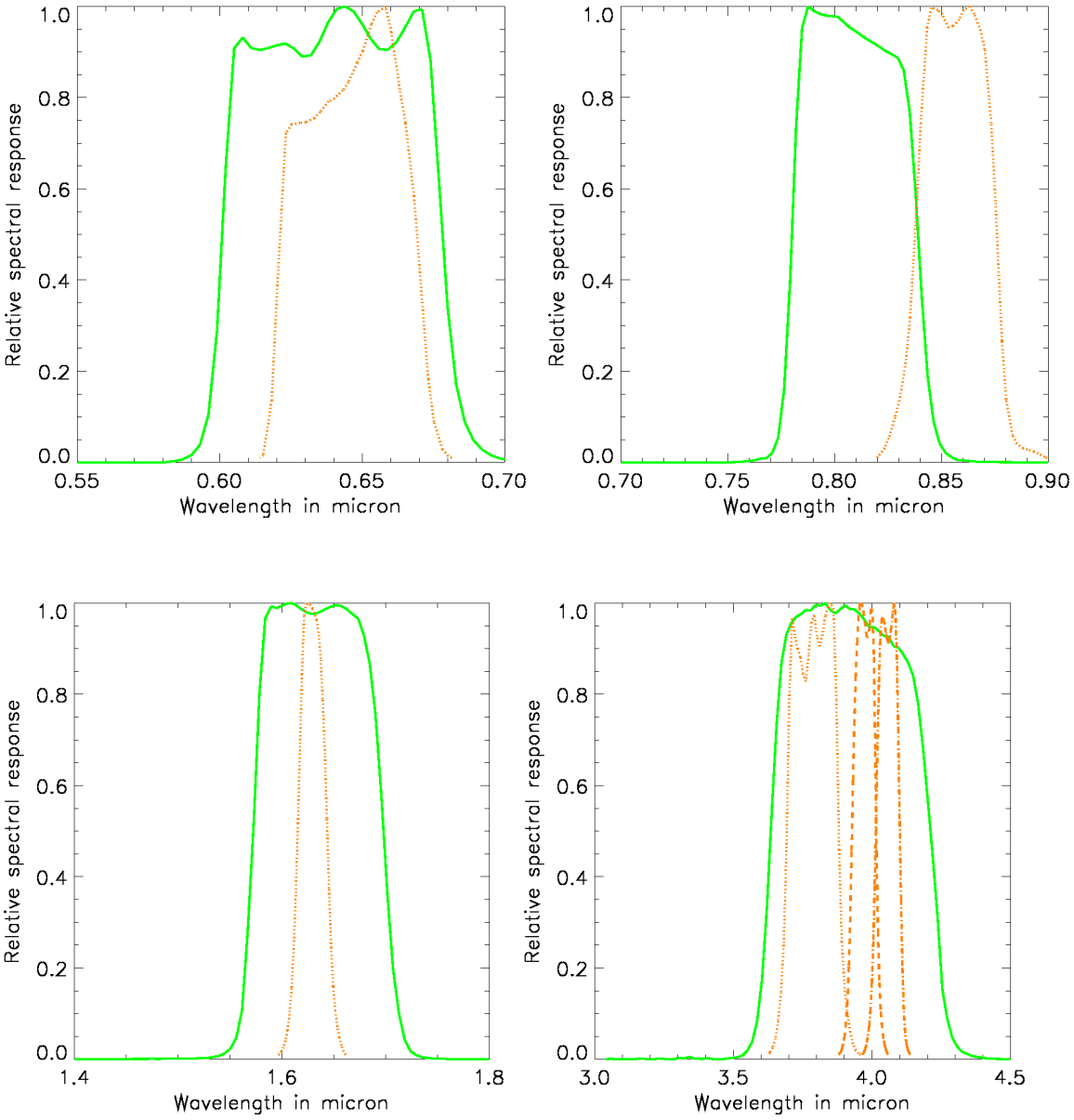

MSG IR3.9 is compared to MODIS channels 20, 22 and 23

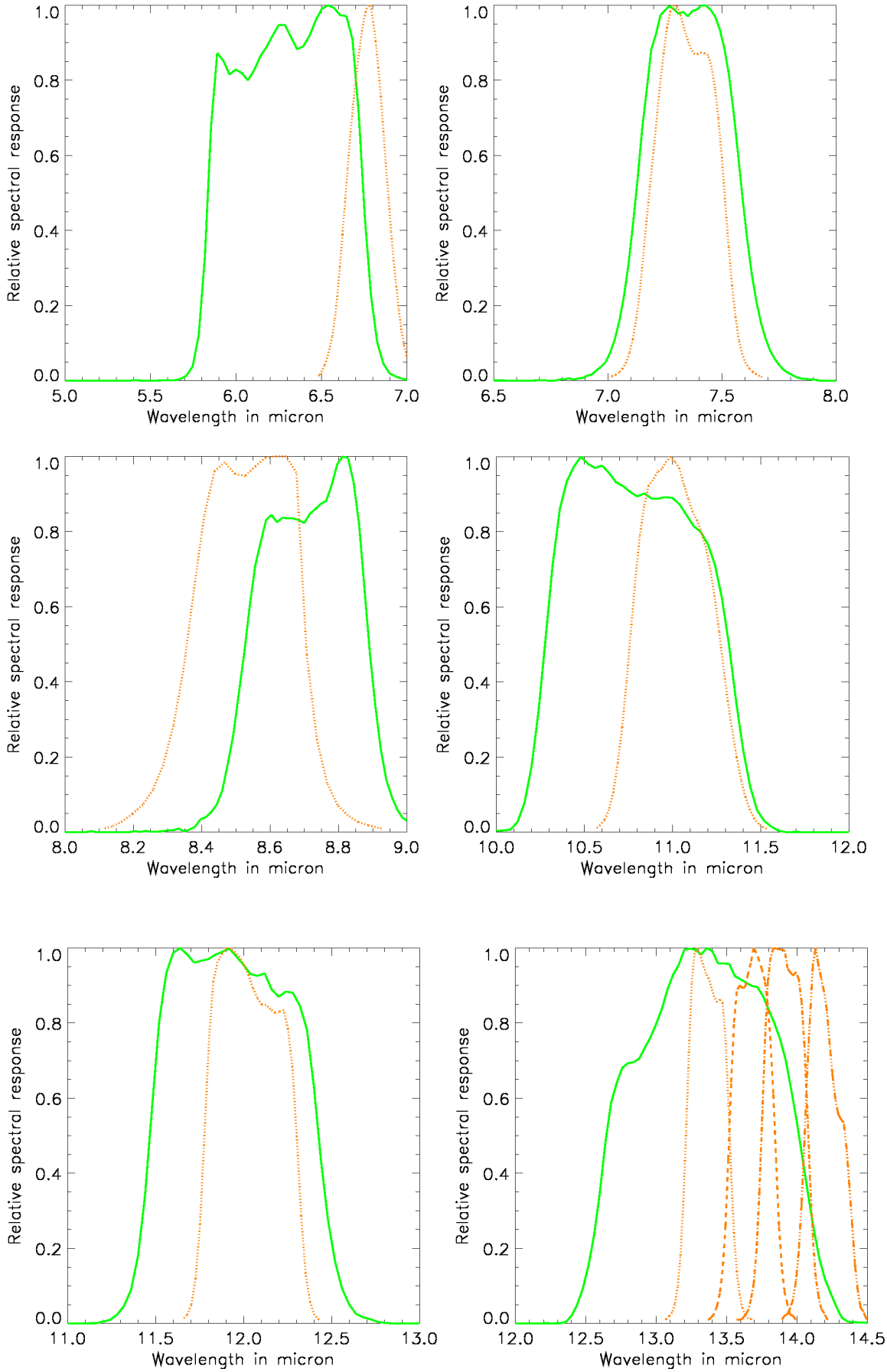

MSG IR13.4 is compared to MODIS channels 33, 34, 35 and 36

The weighting functions obtained for MODIS (brown) and SEVIRI (green) using a mid-latitude summer atmosphere are compared in the following figures. They are useful to estimate the impact of the difference in the spectral response of two MODIS and SEVIRI similar channels on the atmospheric attenuation, especially for sounding channels.

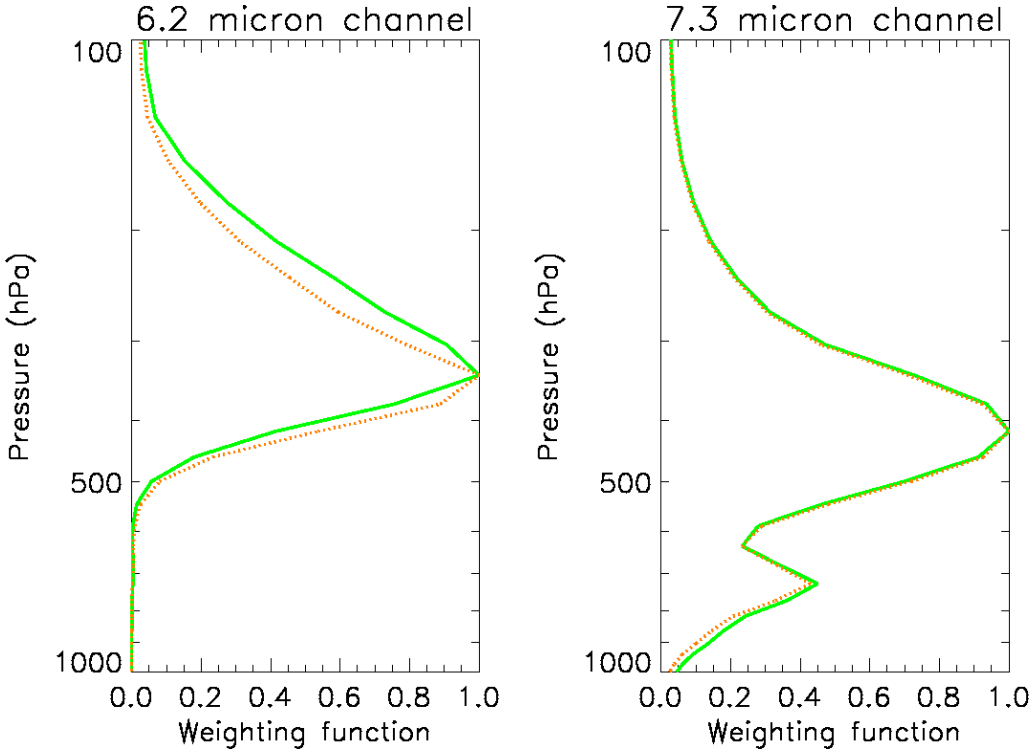

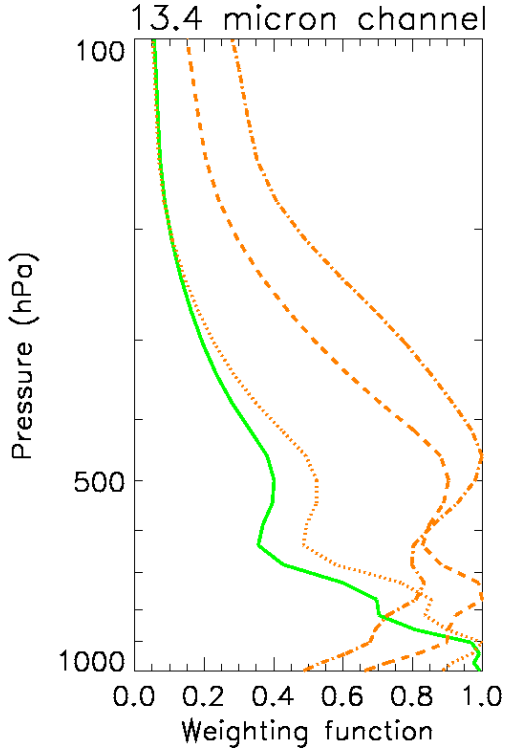

MSG IR13.4 is compared to MODIS channels 33 (dot), 34 (dash) and 35 (dash-dot)

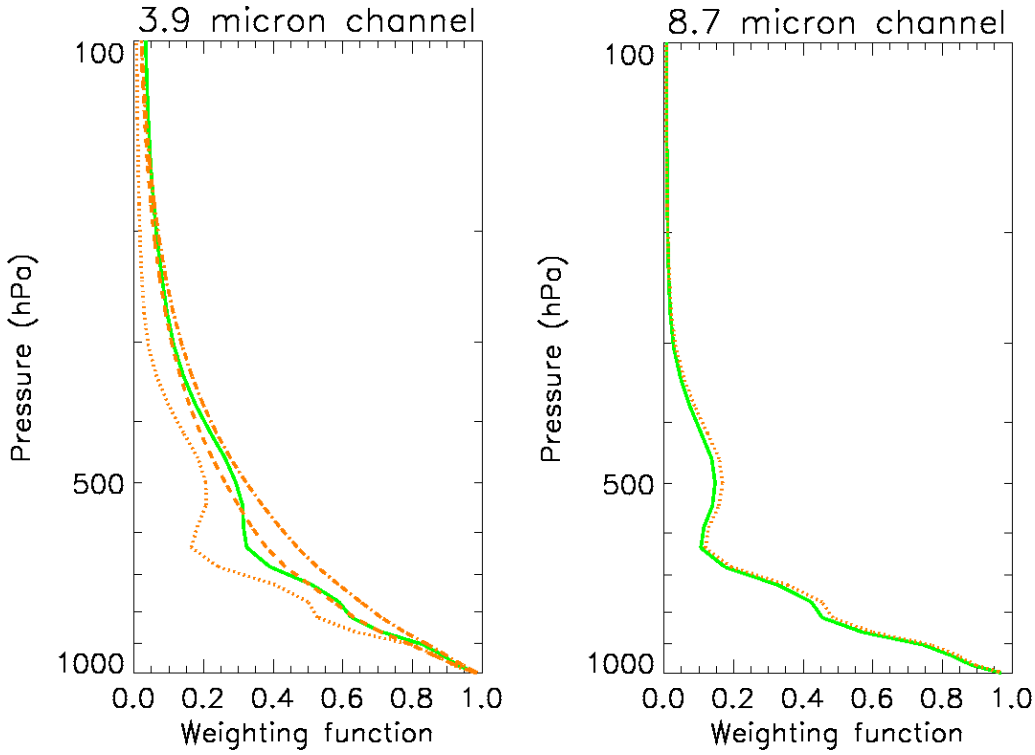

MSG IR3.9 is compared to MODIS channels 20 (dot), 22 (dash) and 23 (dash-dot)

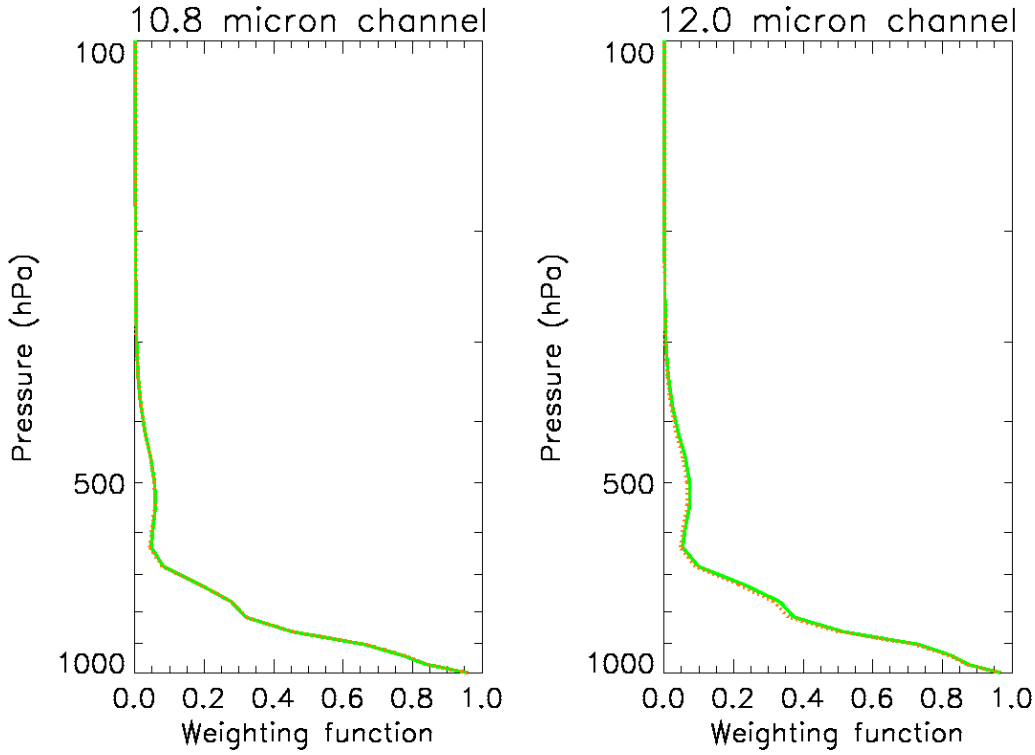

The impact of the different spectral behaviour of MODIS and MSG equivalent channels will be accounted for during the study.

MODIS imagery have been (or will be) used in several ways:

- For visualisation
- For manual extraction of targets (called interactive targets) corresponding to various cloud and surface types (see annex 3 of Ref [1]). 90 MODIS images have been analysed, leading to more than 7600 targets.
- For testing of cloud software modules (will be slightly adapted to be interfaced to MODIS imagery)

In the document, the following labelling of the MODIS channels has been chosen, to allow an easy comparison with SEVIRI imagery.

MODIS channel number	Central wavelength (micron)	Labelling
1	0.65	R0.6µm
2	0.86	R0.8µm
5	1.63	R1.6µm
20	3.79	T3.7µm
22	3.97	T3.9µm
23	4.06	T4.0µm
29	8.53	T8.7µm
31	11.02	T10.8µm
32	12.03	T12.0µm

3. SIMULATION OF CLOUDFREE 8.7µM BRIGHTNESS TEMPERATURES

The SEVIRI cloud detection scheme designed during the development phase includes a threshold test applied to the T8.7µm–T10.8µm brightness temperature difference. This test aims at detecting thin cirrus, and low clouds over arid continental areas. The thresholds used in this test are derived from look-up tables computed off-line using RTTOV applied to the set of TIGR-2 atmospheric profiles. For more details see Ref [2]. No satellite data was available to test and tune this test during the development phase.

Interactive targets have been extracted from 90 MODIS images, corresponding to cloud free ocean and continental areas, and various clouds. They have been used to analyse the impact of using the 8.7 micrometer channel in the cloud detection scheme, and to check the quality of the test that had been devised during the development phase, only relying on simulated data.

It can be seen from figure 3.1 that the T8.7µm–T10.8µm brightness temperature differences should allow to distinguish thin cirrus clouds from cloud free surfaces (oceanic or continental). In fact thin cirrus clouds are characterised by high T8.7µm–T10.8µm values, up to 4-5 degrees, whereas cloud free surfaces present negative values. Figure 3.2 also indicates that T8.7µm–T10.8µm should be more efficient to detect thin ice clouds than T10.8µm–T12.0µm. It can also be concluded from figure 3.1 that T8.7µm–T10.8µm does not usually allow the detection of low clouds, except over arid surfaces characterised by very low T8.7µm–T10.8µm (as shown by figure 3.3).

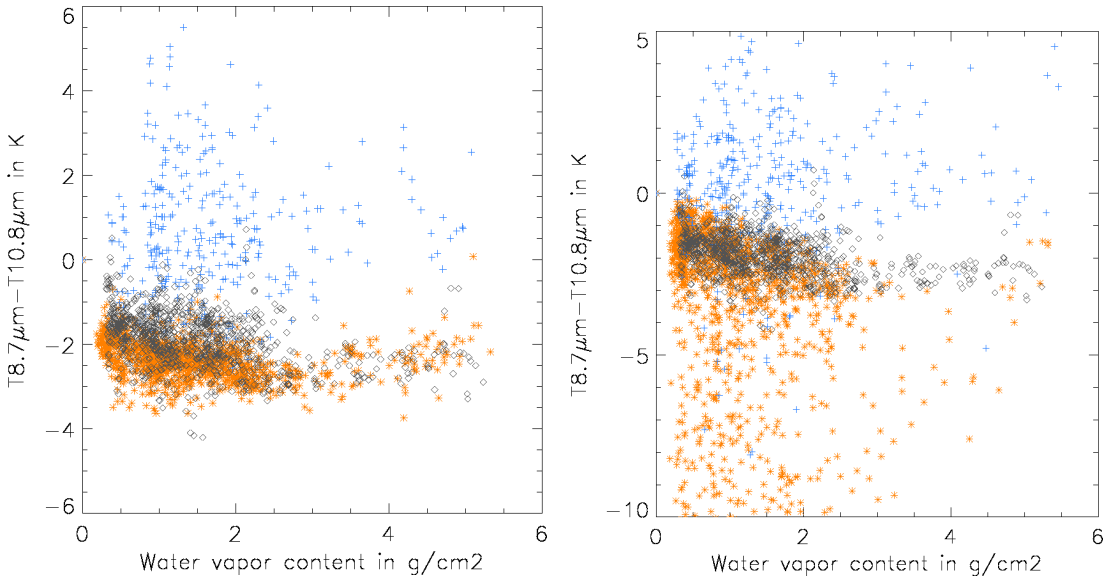

Figure 3.1 Variation of T8.7µm-T10.8µm brightness temperature difference with integrated atmospheric water vapour (nighttime and daytime measurements). For cloud free surface (brown *), low clouds (black diamond) and high thin clouds (blue +)
Left (over ocean), right (over continent).

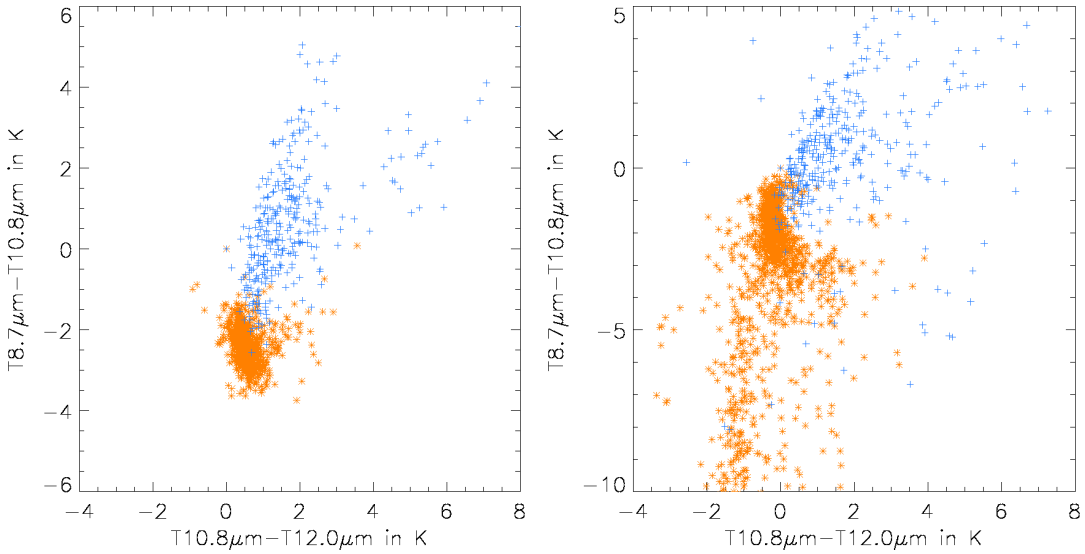

Figure 3.2 Variation of T8.7µm-T10.8µm brightness temperature difference with T10.8µm-T12.0µm brightness temperature difference (daytime and nighttime measurements). For cloud free surface (brown *) and high thin clouds (blue +)
Left (over ocean), right (over continent).

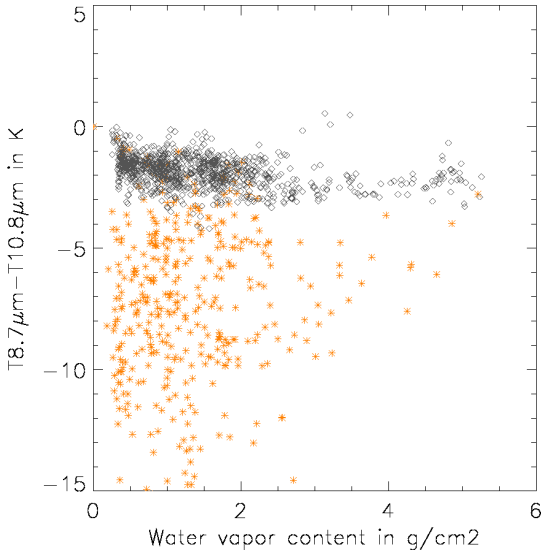

Figure 3.3 Variation of T8.7µm-T10.8µm brightness temperature difference with integrated atmospheric water vapour (daytime and nighttime measurements).
For cloud free arid continental surface (brown *) and low clouds clouds (black diamond).

Cloud free T8.7µm–T10.8µm brightness temperature differences are a function of integrated atmospheric water vapour content (as can be seen on figure 3.4), and also of surface reflectance over the continent, where very highly negative T8.7µm–T10.8µm values can be observed for arid areas (see figure 3.5). The dependency on the satellite viewing angles has not been analysed with MODIS data, as targets corresponding to high viewing angles have not been extracted from the images, due to reported calibration problems in pass edges. These behaviours should be reproduced by the thresholds.

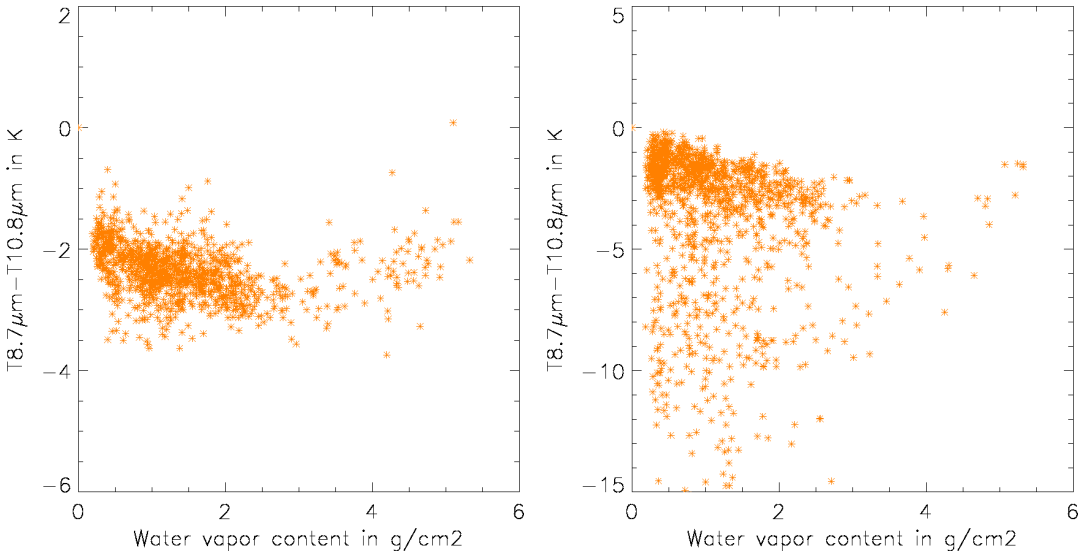

Figure 3.4 Variation of T8.7µm-T10.8µm brightness temperature difference with integrated atmospheric water vapour (nighttime and daytime measurements) for cloud free surface.
Left (over ocean), right (over continent).

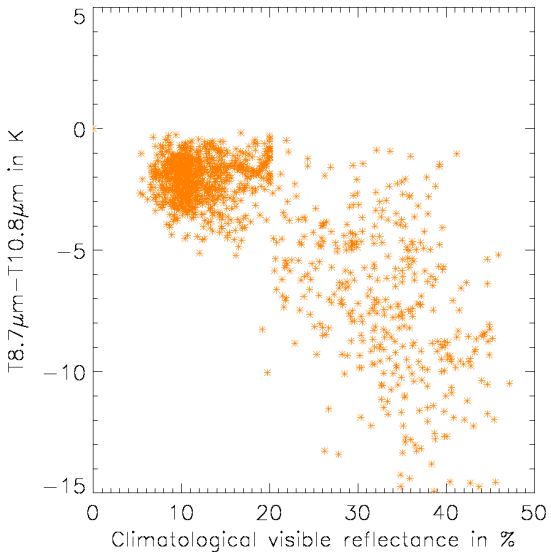

Figure 3.5 Variation of T8.7µm-T10.8µm brightness temperature difference with climatological visible reflectances (nighttime and daytime measurements) for cloud free continental surface.

Figure 3.6 presents the T8.7µm–T10.8µm thresholds tuned to MODIS (from EOS-terra) spectral characteristics. They have been pre-computed by applying RTTOV-6 to radiosondes from dataset made available by ECMWF (see Ref [5]). This dataset contains much more moist atmospheric profiles than TIGR-2, and is therefore better suited for the computation of thresholds valid in all atmospheric conditions.

These thresholds have been compared to T8.7µm–T10.8µm measurements to check the thresholds's efficiency. Results of this comparison are summarized in figures 3.7 and 3.8.

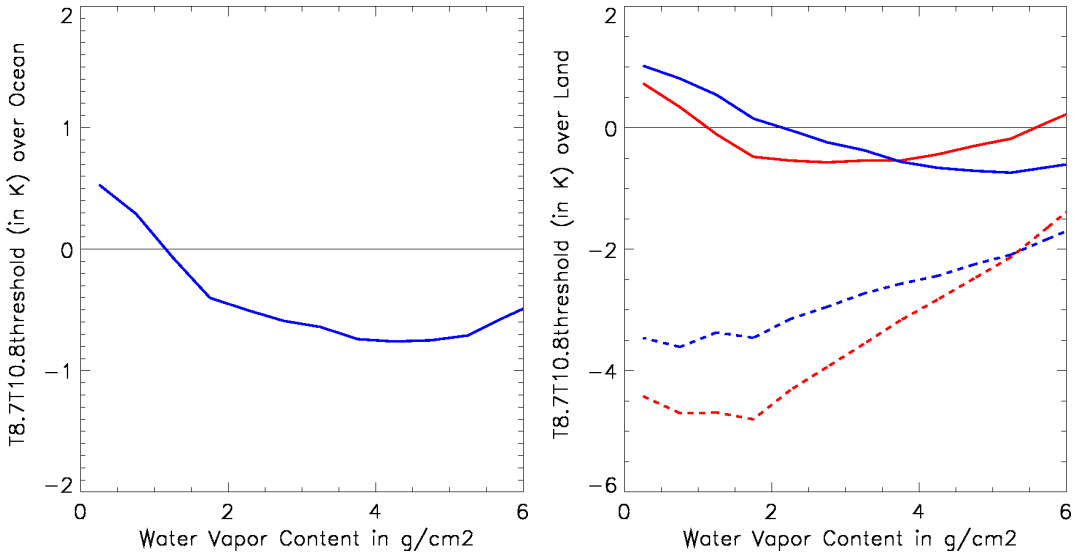

Figure 3.6 Illustration of T8.7µm-T10.8µm threshold at satellite nadir.
Over land, dashed and solid curves correspond to desertic and vegetated areas, blue and red curve to night and daytime conditions.

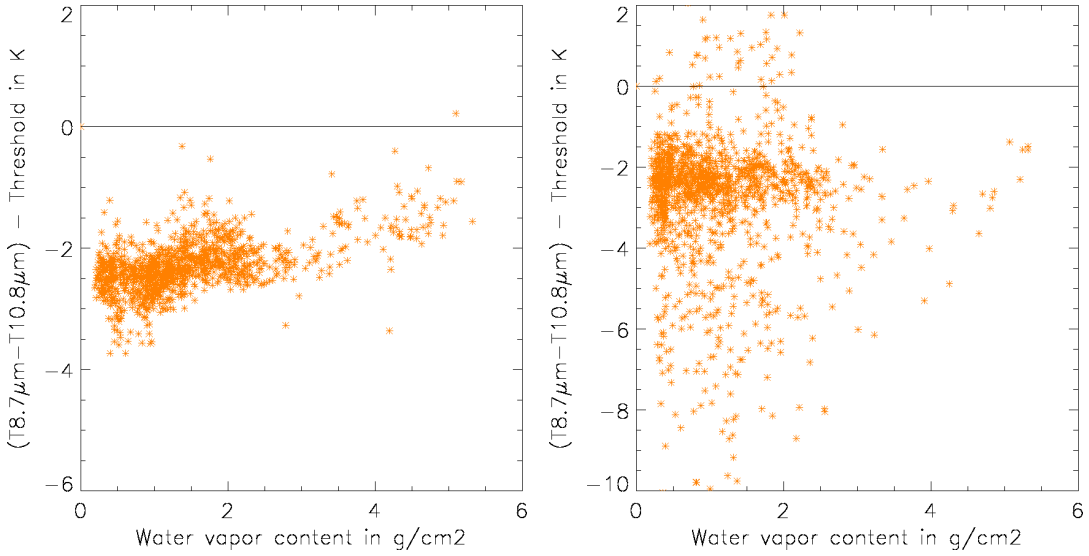

Figure 3.7 Comparison of cloud free T8.7µm-T10.8µm and associated threshold as a function of integrated atmospheric water vapour (nighttime and daytime measurements).
Left (over ocean), right (over continent).

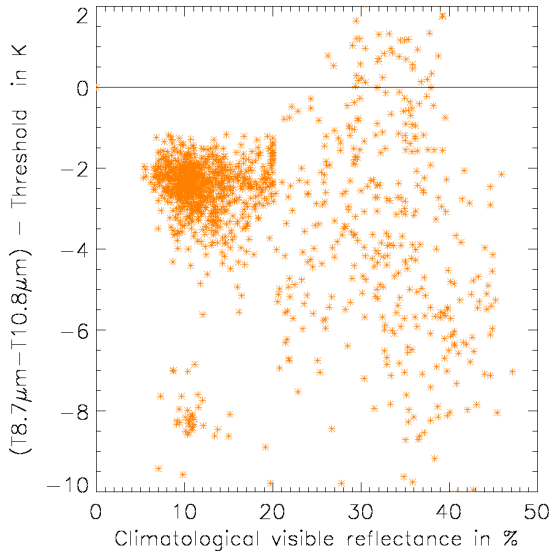

Figure 3.8 Comparison of continental cloud free T8.7µm-T10.8µm and associated threshold as a function of climatological visible reflectance (nighttime and daytime measurements).

We can be rather confident in the quality of the threshold that has been implemented in the SEVIRI CMa software. Nevertheless, the following improvements (tuned with MODIS imagery, see figure 3.9) will be tested when SEVIRI images are available:

- The thresholds applied to T8.7µm–T10.8µm can be generally slightly more severe. In fact we added a 1°C offset to RTTOV simulation for security (as we had no real satellite data to check the 8.7 simulation). It appears that this offset could be reduced.
- The slight dependency on the atmospheric water vapour content observed in the difference between the threshold and the measurements (see figure 3.7) could be reduced by modifying the contrast between the air and the surface temperatures used in the RTTOV simulations.
- The thresholds should be slightly increased for high albedo surfaces to reduce some errors observed in arid areas (see figure 3.8).

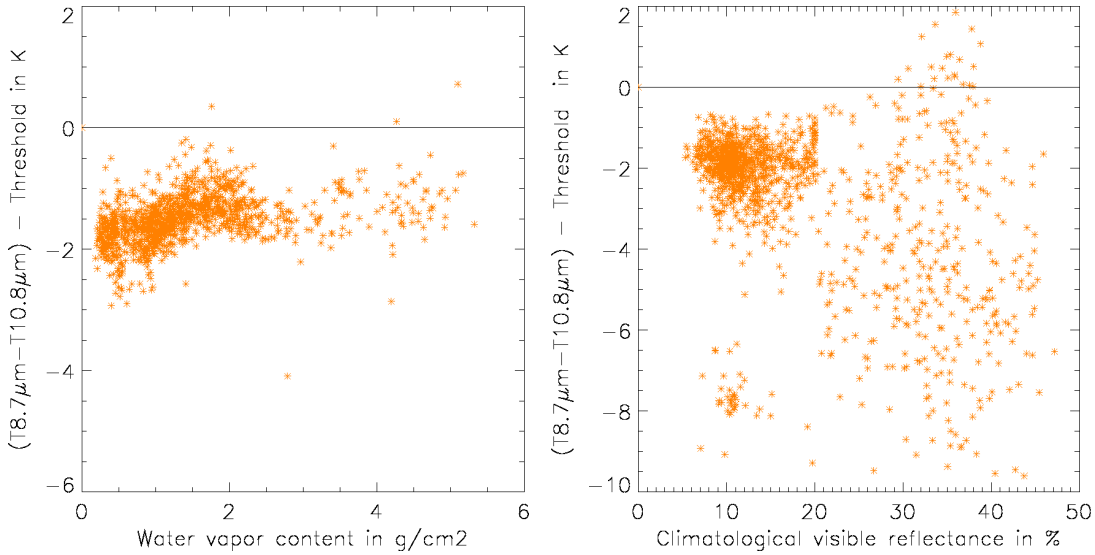

Figure 3.9 Same as 3.7 and 3.8, but with tuned thresholds.

4. NIGHTTIME LOW CLOUD DETECTION: IMPACT OF 3.9µM CHANNEL FILTERS'S WIDTH

Unlike AVHRR or GOES imagery, the SEVIRI 3.9µm channel's filter is large and spreads far beyond 4 micron. This could have an negative effect on the nighttime low clouds detection, as suggested by figure 4.1: the contrast between cloud free surfaces and low clouds in the T10.8µm-T3.9µm feature is much lower if MODIS channel 23 (4.05µm) is used instead channel 20 (3.75µm).

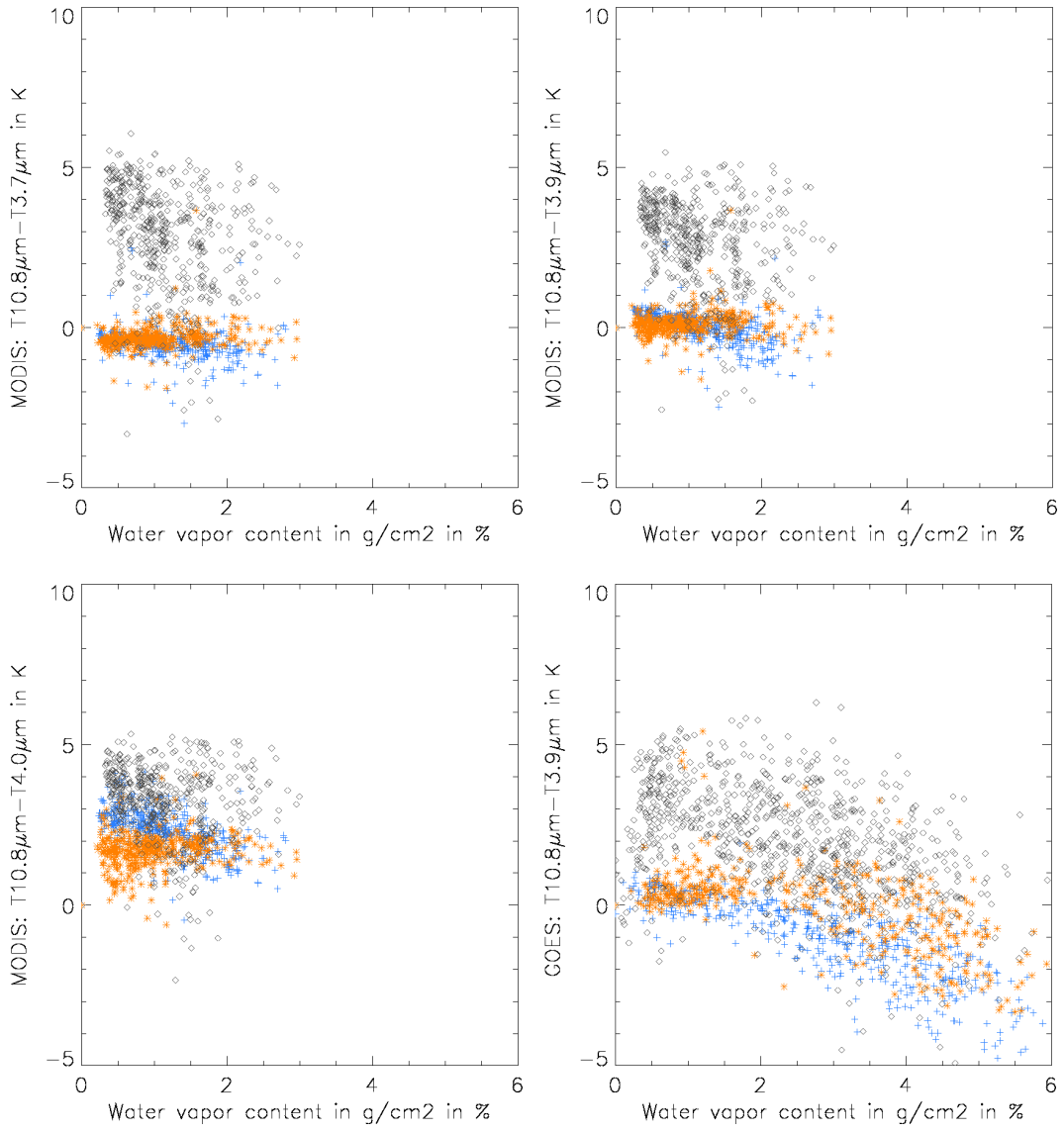

Figure 4.1 Illustration of nighttime low cloud detection using T10.8µm-T3.9µm from MODIS and GOES. Top left: MODIS channel 20 (3.79µm) used, top right: MODIS channel 22 (3.97µm) used; bottom left: MODIS channel 23 (4.05µm) used; bottom right: GOES imagery. Blue +: cloud free oceanic surfaces; Brown *: cloud free continental surfaces; Black diamond: low clouds (fog, stratus and stratocumulus)

The general increase of the cloud free T10.8µm-T3.9µm feature with 3.9µm wavelength (due to the N_2 attenuation beyond 3.85µm) and its variation with water vapour are rather well simulated with RTTOV-6, as can be seen by comparing figures 4.1 and 4.2.

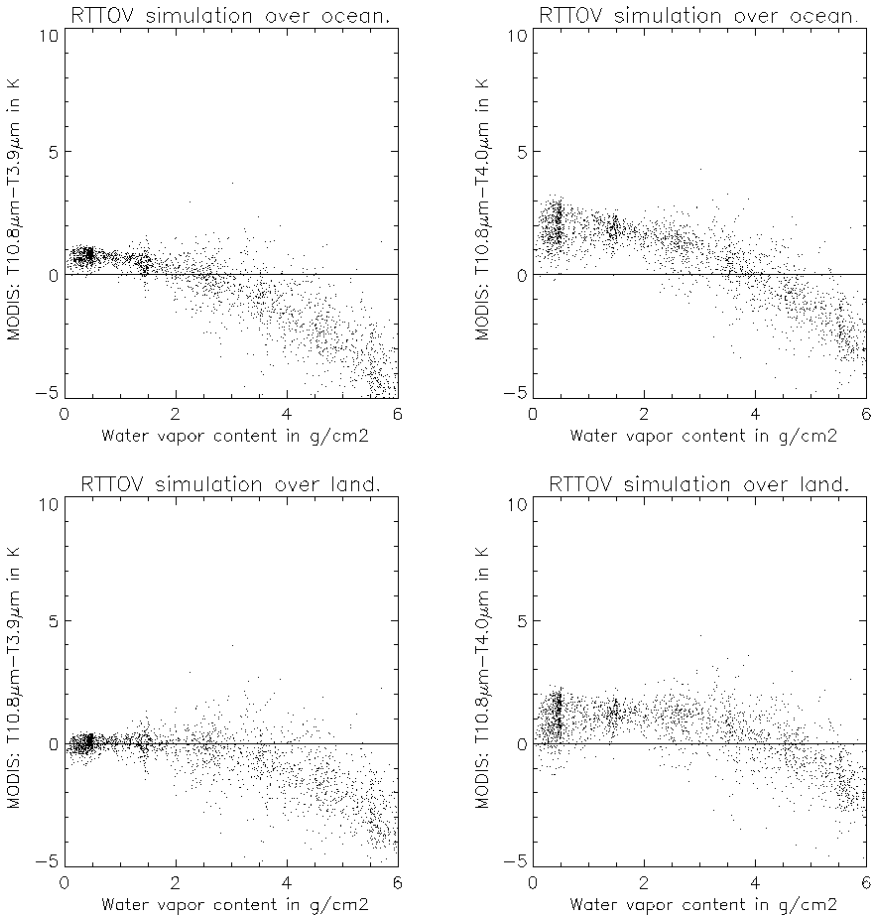

Figure 4.2 RTTOV-6 simulation of MODIS cloud free oceanic and continental T10.8µm-T3.9µm and T10.8µm-T4.0µm using ECMWF radiosondes dataset (see Ref [5]).

The spectral variation of cloudy T10.8µm-T3.9µm with the 3.9µm wavelength is illustrated on figure 4.3. Its analysis, which should take into account atmospheric attenuation (depending on the cloud height) and cloud emissivity (depending on cloud droplets size…), has not been done.

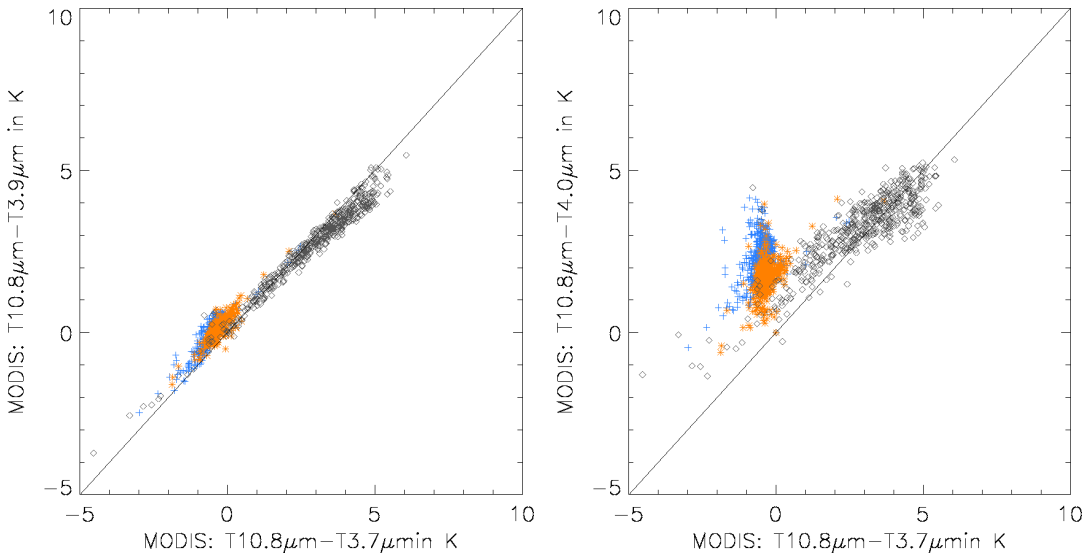

Figure 4.3 Comparison of nighttime T10.8µm-T3.9µm with MODIS 20 (3.79µm), MODIS 22 (3.97µm) and 23 (4.05µm). Blue +: cloud free oceanic surfaces; Brown *: cloud free continental surfaces; Black diamond: low clouds (fog, stratus and stratocumulus)

SEVIRI cloud free and cloudy measurements have been simulated from the MODIS measurements displayed in figure 4.1. We additionally accounted for the CO_2 attenuation beyond 4.15µm (not present in MODIS channels) which should be slightly stronger for cloud free surfaces than for clouds (due to the longer geometrical path), thus decreasing the contrast between cloud free surfaces and low clouds in the T10.8µm-T3.9µm feature.

SEVIRI 3.9µm filter has been split in three parts: [3.5-3.9], [3.9-4.01] and [4.01-4.5] located around MODIS channel 20, 22 and 23. Radiances are first computed in these three spectral bands using the brightness temperatures in MODIS channel 20, 22 and 23 and the spectral response of the SEVIRI filter; these three radiances are added and the result is transformed into brightness temperatures using the SEVIRI filter. Results of this simulation are presented in figure 4.4 (left). To estimate the CO_2 absorption beyond 4.15µm (not present in the previous simulation), we additionally substract 6°C (5°C for cloudy targets) to the MODIS channel 23 brightness temperatures before computing the radiance in the [4.01-4.5] part of the SEVIRI filter [These values (6°C and 5°C) have been estimated applying MODTRAN 3.5 Radiative Tranfer Model to mid latitude summer atmosphere assuming a cloud at 2km and satellite at nadir]. Results of this second simulation (presented in figure 4.4 and 4.5 (right)) indicates that the CO_2 absorption should induce a small (less than 0.5°C) additional decrease of the contrast between cloud free surfaces and low clouds in the SEVIRI T10.8µm-T3.9µm feature.

This study indicates that the contrast between cloud free surfaces and low clouds in the SEVIRI T10.8µm-T3.9µm feature should be lower by about one degree from what is observed with GOES imagery or MODIS channel 22, indicating a slight degradation of its ability to detect low clouds at nighttime.

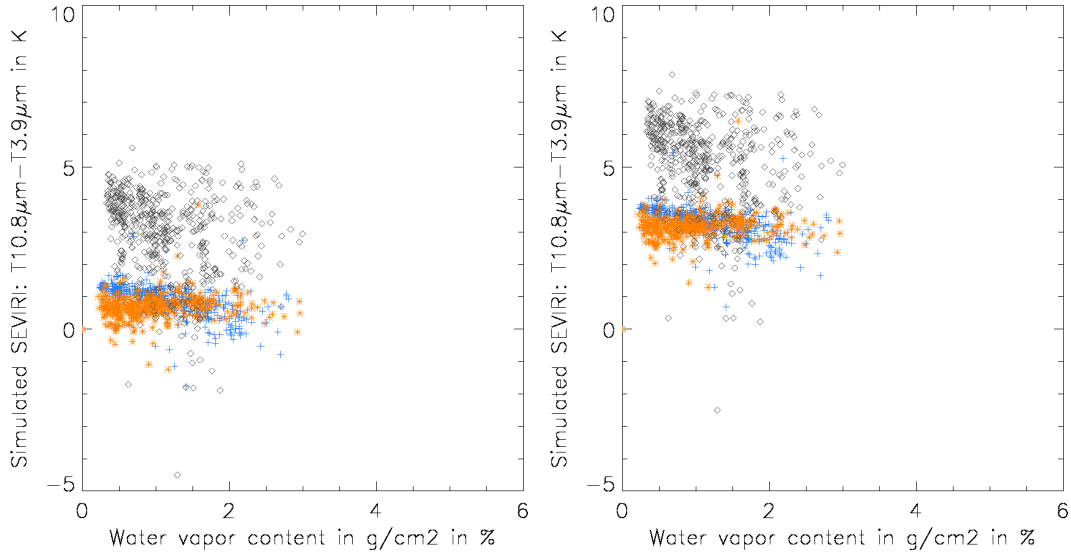

Figure 4.4 Illustration of nighttime low cloud detection using SEVIRI T10.8µm-T3.9µm simulated using MODIS channels 20, 22, 23 and 31 (additional CO_2 attenuation beyond 4.15µm is accounted for in the SEVIRI simulations on the right side).
Blue +: cloud free oceanic surfaces; Brown *: cloud free continental surfaces; Black diamond: low clouds (fog, stratus and stratocumulus)

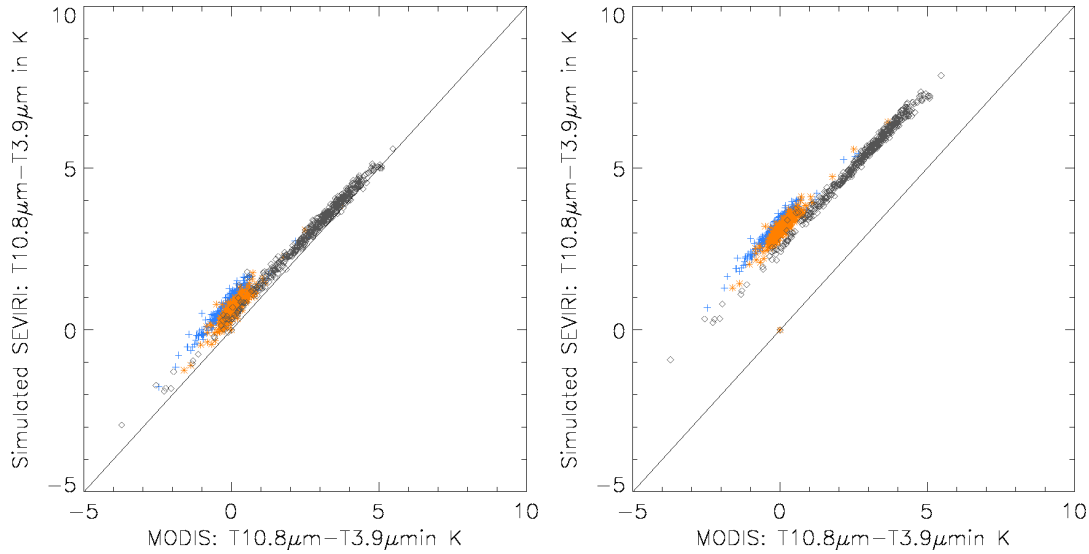

Figure 4.5 Comparison of simulated SEVIRI and MODIS T10.8µm-T3.9µm (additional CO_2 attenuation beyond 4.15µm is accounted for in the SEVIRI simulations on the right side). Blue +: cloud free oceanic surfaces; Brown *: cloud free continental surfaces; Black diamond: low clouds (fog, stratus and stratocumulus)

5. NIGHT-TIME LOW CLOUDS DETECTION: IN ARID AREAS

At night-time, low clouds are usually characterized by their T10.8µm-T3.9µm brightness temperature difference which is usually higher that of the oceans or continental surfaces. This is not true over desertic areas which may also exhibit high T10.8µm-T3.9µm brightness temperature difference, as can be seen on figure 5.1 (left). Figure 5.1 and 5.2 clearly shows that the nighttime low clouds detection test can be easily improved by adding a simple test of the T8.7µm-T10.8µm brightness temperature difference.

The test, presently used in the SEVIRI algorithm, will be modified as follows:

A pixel is classified as cloudy if

- T10.8µm-T3.9µm > T10.8T3.9threshold
- T8.7µm-T10.8µm > -4°C or T10.8µm-T12.0µm > -0.5°C

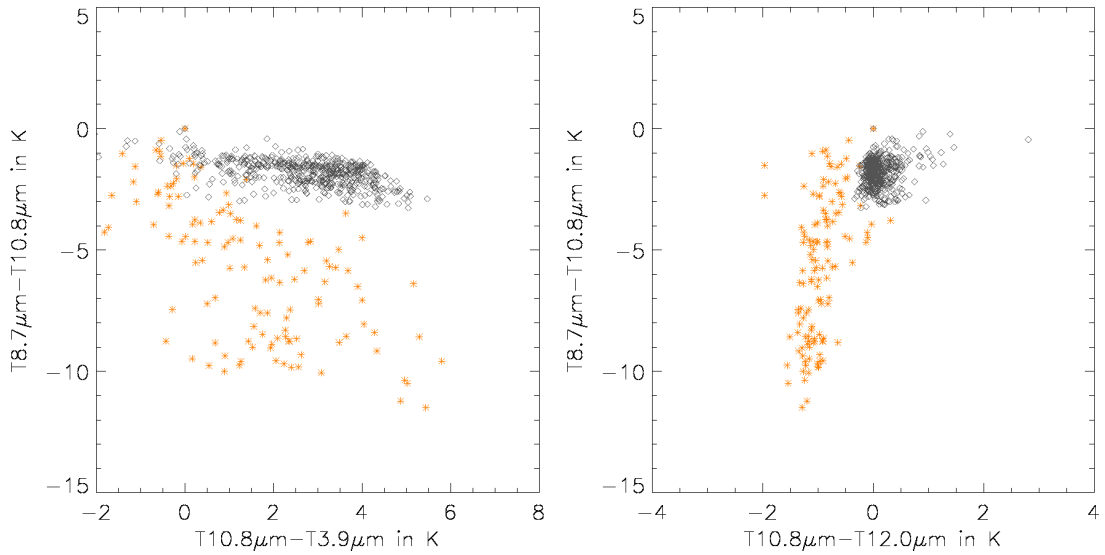

Figure 5.1 Variation of T8.7µm-T10.8µm brightness temperature difference with T10.8µm-T3.9µm (left) and T10.8µm-T12.0µm (right) (nighttime measurements).
For cloud free arid continental surface (brown *) and low clouds clouds (black diamond).

6. NIGHT-TIME LOW CLOUD DETECTION: IN WARM SECTOR

At nighttime over continental areas, some low clouds are very difficult to detect with the test applied to T10.8µm-T3.9µm brightness temperature difference. These situations have been observed with AVHRR imagery over France; they correspond generally to stratocumulus layers invading western Europe, inside warm sectors, with rain or drizzle. MODIS imagery corresponding to situations where such clouds were identified in AVHRR have been desarchived to be analysed.

An empirical test combining T10.8µm-T3.9µm and T10.8µm-T12.0µm had been proposed during the prototyping phase with GOES imagery, but was not very successful and too empirical to be easily applied to SEVIRI imagery. We used MODIS imagery to check whether the 8.7µm and 13.4µm channels could contribute to the low cloud detection.

Figures 6.1 clearly indicate that no improvement in the nighttime low cloud detection above vegetated areas can be expected from the use of 8.7µm or 13.4µm.

The empirical test combining T10.8µm-T3.9µm and T10.8µm-T12.0µm will be removed. Instead we will implement a test that simultaneously thresholds T10.8µm, T10.8µm-T3.9µm and T10.8µm-T12.0µm brightness temperatures using more severe thresholds than the ones used in the individual tests. This can be seen as desperate attempt to improve the detection of low clouds at nighttime.

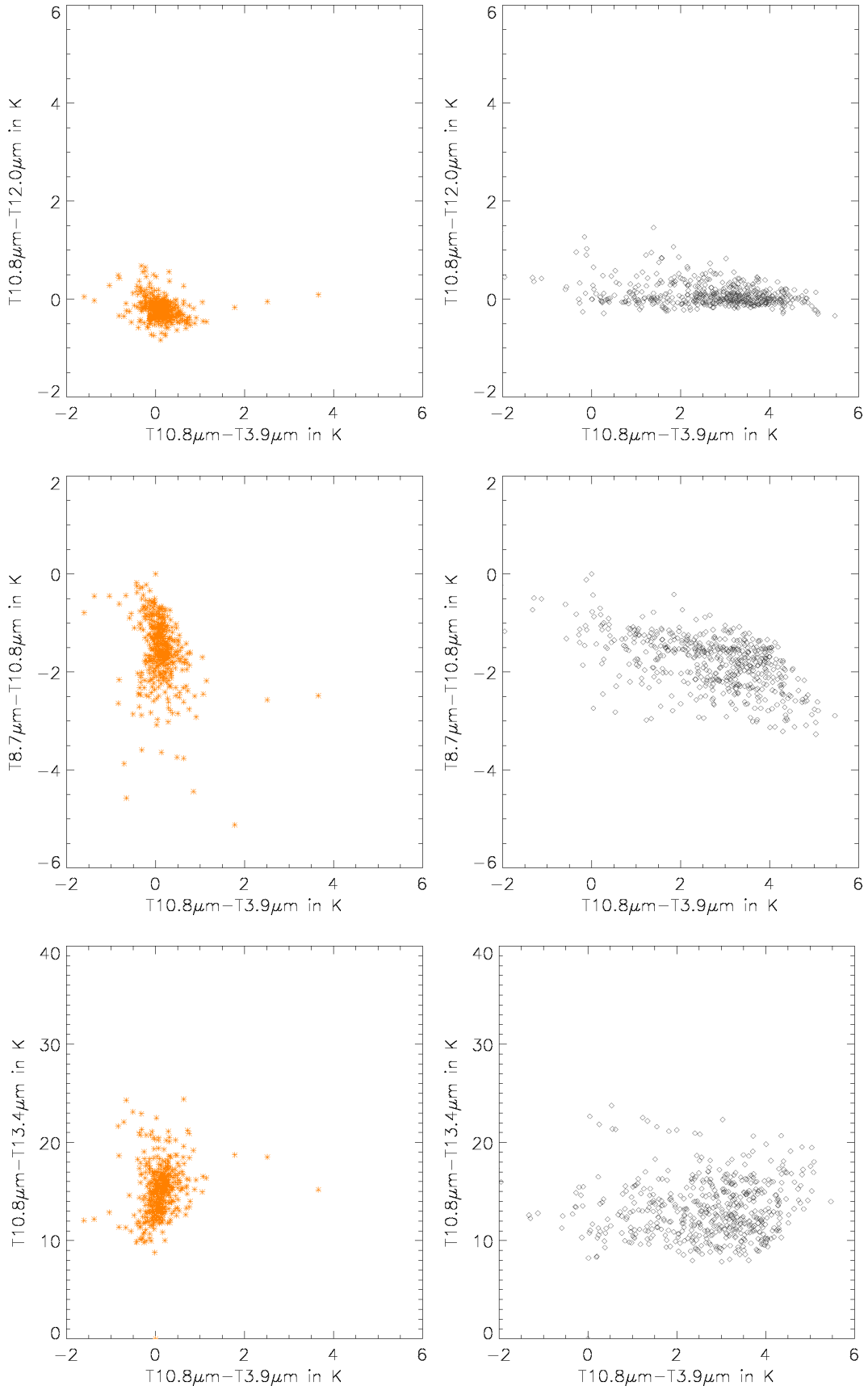

Figure 6.1 Illustration of nighttime low cloud detection over vegetated areas using T10.8µm-3.90µm, T10.8µm-T12.0µm, T8.7µm-T10.8µm, T10.8µm-T13.4µm. On the left side: cloud free vegetated surfaces (brown *); on the right side: low clouds (fog, stratus and stratocumulus) (Black diamond)

7. DISTINCTION BETWEEN SUB-PIXEL LOW CLOUDS AND THIN CIRRUS

In the SEVIRI cloud classification scheme designed during the development phase, it may happen that the thinnest cirrus clouds are mis-classified as sub-pixel low clouds, and even worse as low clouds (in the daytime scheme). This paragraph intends to illustrate how the new channels available on SEVIRI (the 1.6µm reflectance and the 8.7µm brightness temperature) could contribute to a better classification of cirrus and sub-pixel low clouds.

Figure 7.2 clearly indicates that the R1.6µm reflectance will not contribute to improve the classification of cirrus clouds. On the other hand, the 8.7µm brightness temperature (combined with the 10.8µm brightness temperature) seems rather efficient to separate thin cirrus clouds from low clouds or small cumulus (see figure 7.1). Some limitations apply to the use of this channel:

- cold opaque clouds may have similar T8.7µm-T10.8µm values, as cirrus clouds (see figure 7.3);
- thin cirrus over desert may have low negative T8.7µm-T10.8µm values due to the low 8.7µm emissivities of arid surfaces.

The use of 8.7µm channel should therefore only be beneficial to improve the classification of the thinnest cirrus clouds over the ocean and vegetated areas: thin cirrus clouds would then be characterized by high T8.7µm-T10.8µm, which should not be the case for sub-pixel low clouds or low clouds. The cloud type (CT) algorithm will be modified accordingly.

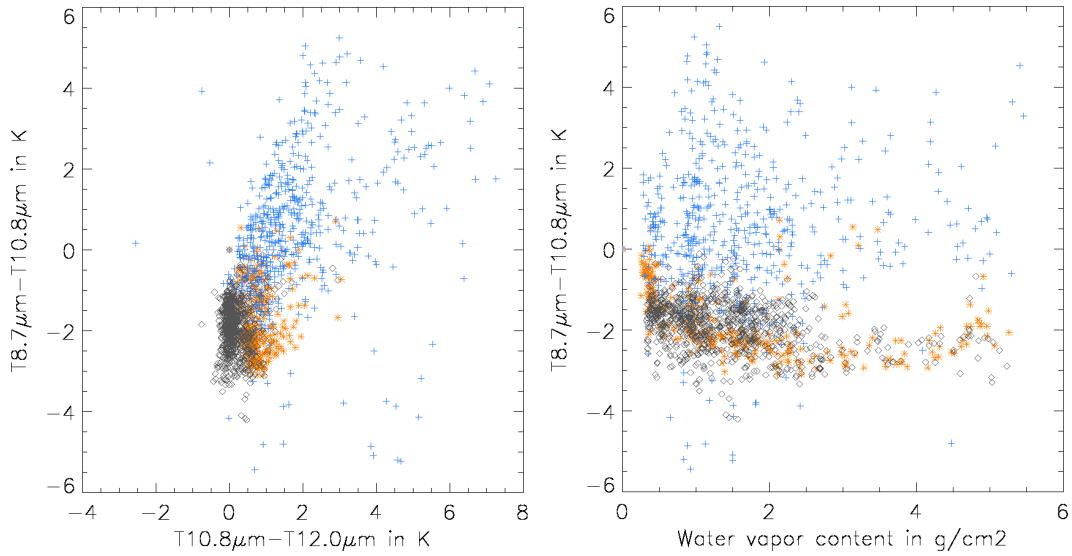

Figure 7.1 Variation of T8.7µm-T10.8µm brightness temperature difference with T10.8µm-T12.0µm brightness temperature difference (left) and integrated atmospheric water vapour content (right) (daytime and nighttime measurements). For low clouds (black diamond), high thin clouds (blue +) and small cumulus (brown *)

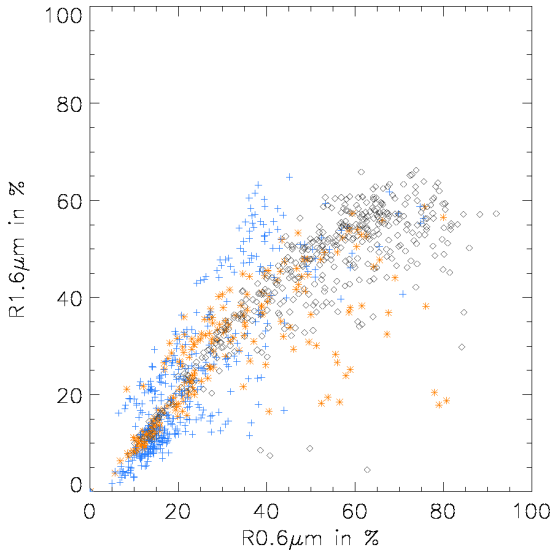

Figure 7.2 Variation of R1.6µm reflectance with R0.6µm visible reflectance. For low clouds (black diamond), high thin clouds (blue +) and small cumulus (brown *)

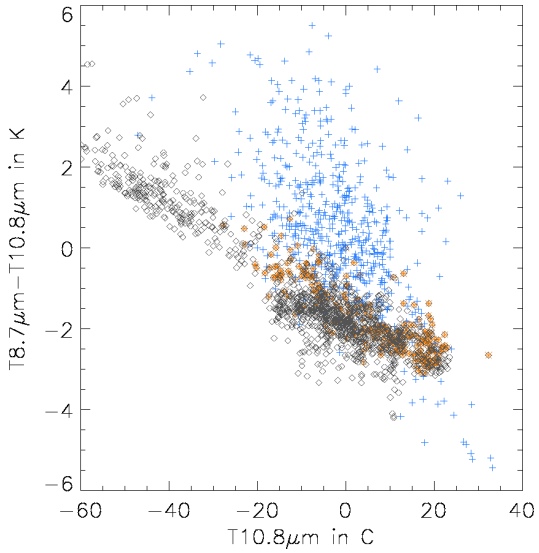

Figure 7.3 Variation of T8.7µm-T10.8µm brightness temperature difference with T10.8µm brightness temperature (daytime and nighttime measurements). For opaque low medium or high clouds (black diamond), high thin clouds (blue +) and small cumulus (brown *)

8. DETECTION OF SNOW

During the development phase, the following algorithm to detect snow at daytime was designed using AVHRR (from NOAA-15, for the 1.6µm channel prototyping) and GOES imagery (see ref [1]):

A pixel is classified as contaminated by snow if :

- R1.6µm < R1.6threshold or (T3.9µm-T11µm)/cos(θsol) < 15°C
- (T10.8threshold - 5°C) < T10.8µm < 4°C
- T10.8µm-T12.0µm < 2°C
- R0.6threshold < R0.6µm
- 20% < R0.8µm

-where R1.6thrshold is a threshold described in Ref[1], T10.8threshold and R0.6threshold are thresholds used in cloud masking with infrared and visible channels, and θsol is the solar zenith angle.
-T3.9µm is used only if R1.6µm is unavailable (solar elevation must then be higher than 20 degrees)

A pixel is classified as contaminated by ice if :

- Climatological SST < 4°C
- R1.6µm < R1.6thrshold or (T3.9µm-T10.8µm)/cos(θsol) < 15°C
- (T10.8threshold - 5°C) < T10.8µm < 4°C
- T10.8µm-T12.0µm < 2°C
- R0.6threshold < R0.6µm
- 20% < R0.8µm

-where R1.6thrshold is a threshold described in Ref[1], T10.8threshold and R0.6threshold are thresholds used in cloud masking with infrared and visible channels, and θsol is the solar zenith angle.
-T3.9µm is used only if R1.6µm is unavailable (solar elevation must then be higher than 20 degrees)

No algorithm was proposed at nighttime.

MODIS imagery has been used to check this daytime algorithm for its final application to SEVIRI and to analyse whether a nighttime algorithm could be considered.

8.1 SNOW AT DAYTIME

The main feature allowing the snow detection is its solar reflection, which is high in the visible spectrum (at 0.6µm or 0.8µm), but low at 1.6µm or 3.9µm. R0.8µm is used to limit the confusion of shadows with snow. T10.8µm -T12.0µm is supposed to decrease the misclassification of thin high clouds with snow. Finally, the thresholding of T10.8µm (and SSTclim) limits the detection of snow in areas not too warm and too cold.

The analysis of targets extracted from MODIS imagery allows the following observations:

- As expected and illustrated in figure 8.1.1, snow is characterized by low values of solar reflection at 1.6µm and 3.9µm (approximated by the T3.9µm-T10.8µm normalized for solar elevation).
- The separation of snow with clouds seems easier to perform using the 1.6µm channel:
  - low clouds (highly reflective in the visible spectrum) may have rather low T3.9µm -T10.8µm brightness temperature difference as snow; this confusion is not observed if 1.6µm reflectances are used.
  - high thin clouds (having rather low visible reflectance) may correspond to low 1.6µm reflectance and could therefore be confused with snow; the additional test applied to T10.8µm -T12.0µm (using a constant threshold set to 2°C) is too rough to limit this misclassification (see figure 8.1.6).
- The threshold value applied to T3.9µm -T10.8µm was set to 15°C, using GOES imagery. Figure 8.1.3 indicates that the threshold should be dependent on the exact spectral filter, as T3.9µm -T10.8µm (normalised from solar elevation) for snow are 10°C lower at 4.0

micron than at 3.7 micron. This must be due to the strong atmospheric absorption (mainly CO_2; see also paragraph 4 in this report) at wavelengths beyond 4 micron, and also to the dependency of snow reflectance with wavelength (a local maximum at around 3.8micron (see Salisbury, 1994) is observed).

- The threshold applied to the R1.6µm reflectance is around 6-7% too low (see figure 8.1.3), which was not observed with the AVHRR of NOAA-15 (see Ref[1]). This discrepancy is not understood. Explanations could be:
  - the different value of the central wavelength: the ice absorption is higher for AVHRR Channel 1.6µm (central wavelength: 1.607) than for MODIS Channel 1.6µm (central wavelength: 1.629) leading to lower reflectance. But the magnitude of this effect should be lower than 6-7%. Note that we can expect similar effect for SEVIRI (see spectral filters in paragraph 2).
  - calibration problems: R0.6µm and R1.6µm reflectances over ocean and land (including arid areas) are coherent for both AVHRR and MODIS, indicating that calibrations problems could not explain the 6-7% differences in snow 1.6µm reflectance between AVHRR and MODIS.
- Moreover, the variation with the angles of the snow 1.6µm reflectance (see figure 8.1.4) is not very well accounted for by the threshold (as shown by figure 8.1.5).

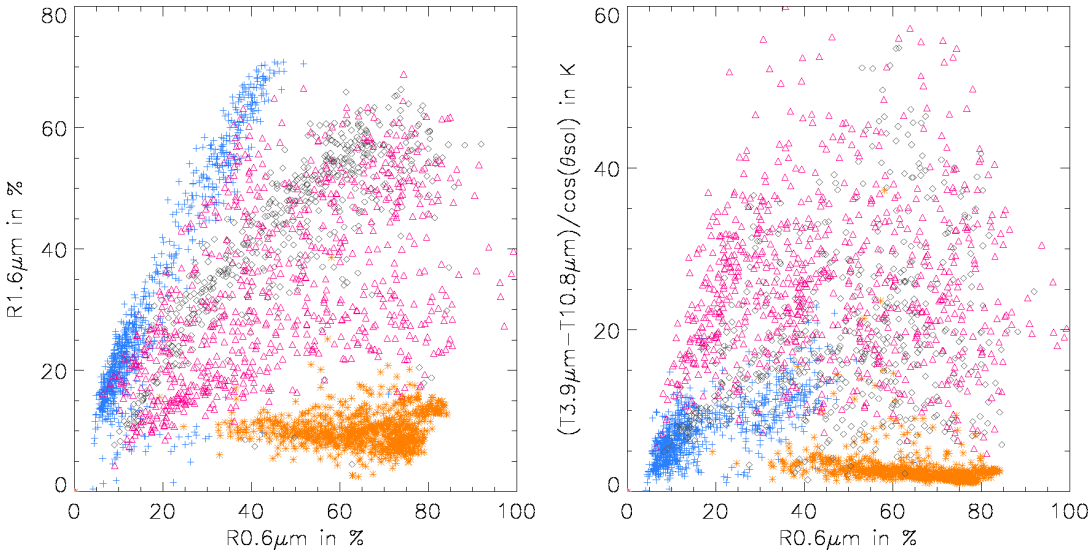

Figure 8.1.1 Variation of R1.6µm reflectance or T3.9µm-T10.8µm brightness temperature difference (normalized for solar elevation) with R0.6µm visible reflectance for cloud free continental surface (blue +), snow (brown *), stratus, stratocumulus or cumulus clouds (black diamond), cirrus (over land or low clouds), cirrostratus, altocumulus and altostratus (purple-coloured triangles).

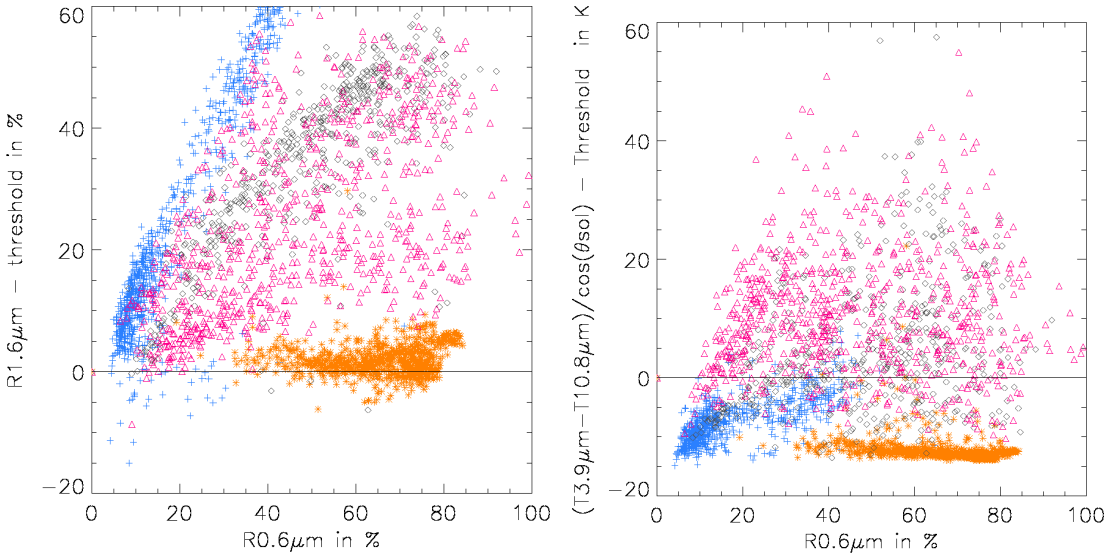

Figure 8.1.2 Variation of R1.6µm reflectance or T3.9µm-T10.8µm brightness temperature difference (normalized for solar elevation) minus the corresponding thresholds with R0.6µm visible reflectance for cloud free continental surface (blue +), snow (brown *), stratus, stratocumulus or cumulus clouds (black diamond), cirrus (over land or low clouds), cirrostratus, altocumulus and altostratus (purple-coloured triangles).

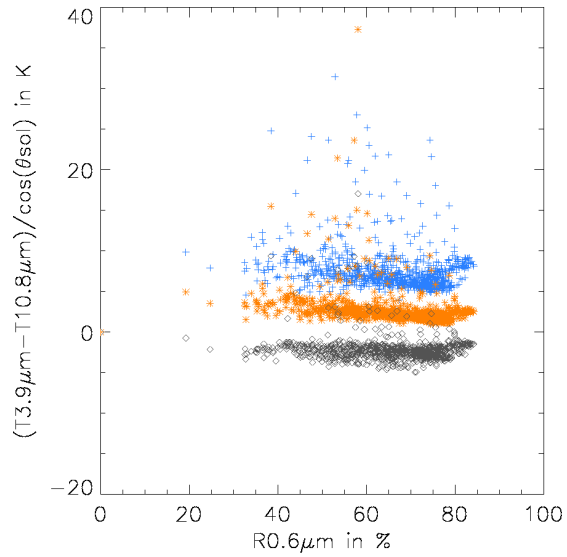

Figure 8.1.3 Illustration of the impact on the spectral filters' width at 3.9µm on the T3.9µm-T10.8µm brightness temperature difference (normalized for solar elevation) for snow targets. Blue +: MODIS channel 20 (3.79µm); Brown *: MODIS channel 22 (3.97µm); Black diamond: MODIS channel 23 (4.05µm)

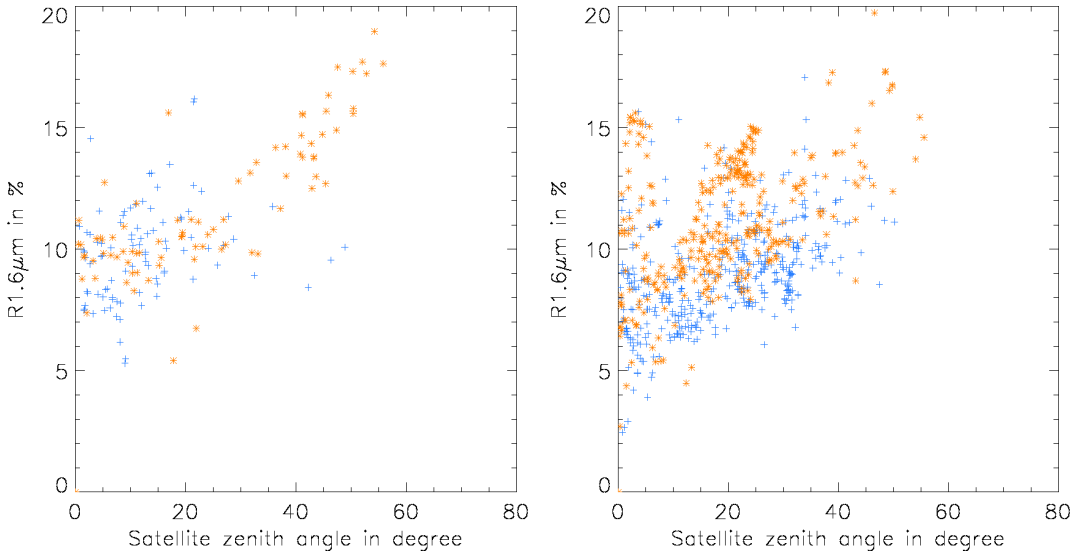

Figure 8.1.4 Variation of R1.6µm reflectance with satellite zenith angles for solar zenith angles lower (left) or higher (right) than 50 degrees. In the forward scatter (brown *) or backward scatter (blue +) direction.

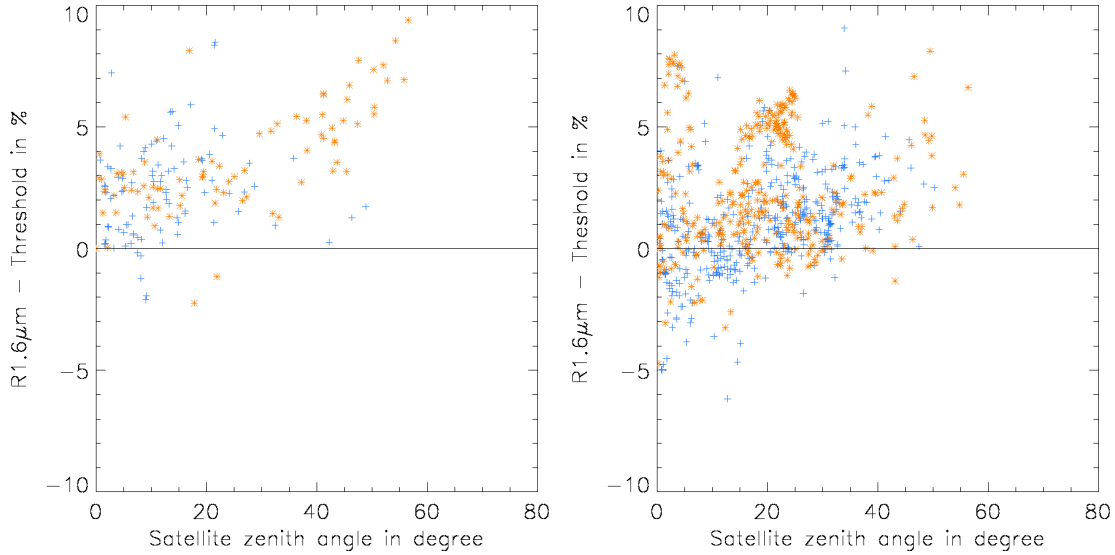

Figure 8.1.5 Variation of R1.6µm reflectance minus the threshold with satellite zenith angles for solar zenith angles lower (left) or higher (right) than 50 degrees. In the forward scatter (brown *) or backward scatter (blue +) direction.

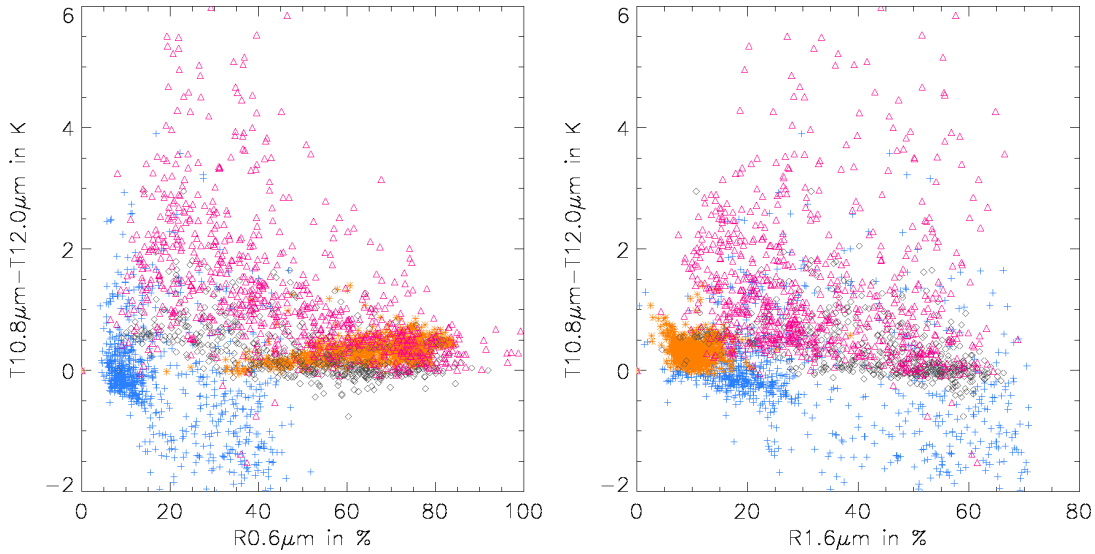

Figure 8.1.6 Variation of T10.8µm-T12.0µm brightness temperature difference with R0.6µm visible reflectance (left) or R1.6µm reflectance (right) for cloud free continental surface (blue +), snow (brown *), stratus, stratocumulus or cumulus clouds (black diamond), cirrus (over land or low clouds), cirrostratus, altocumulus and altostratus (purple-coloured triangles).

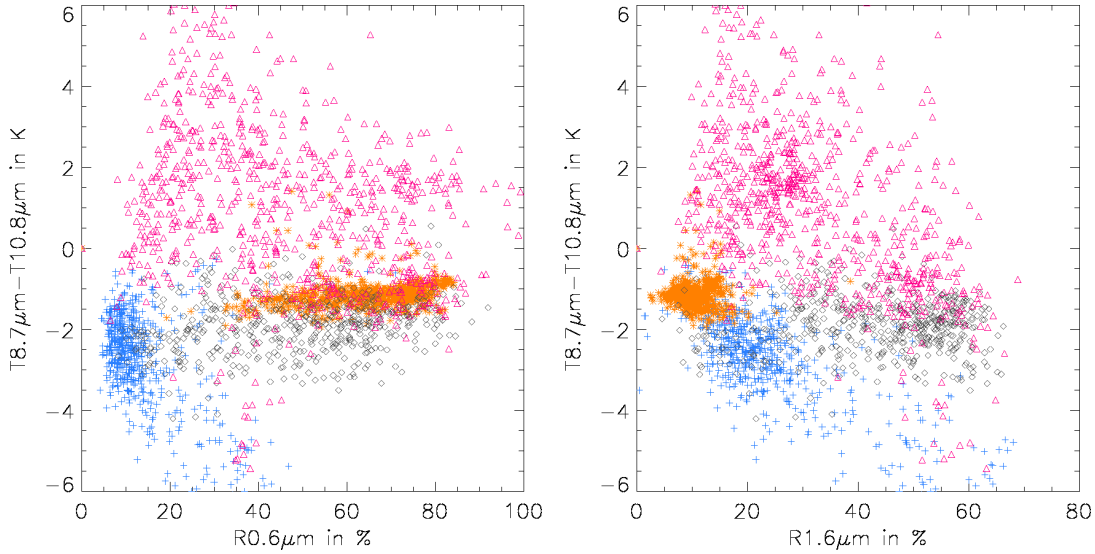

Figure 8.1.7 Variation of T8.7µm-T10.8µm brightness temperature difference with R0.6µm visible reflectance (left) or R1.6µm reflectance (right) for cloud free continental surface (blue +), snow (brown *), stratus, stratocumulus or cumulus clouds (black diamond), cirrus (over land or low clouds), cirrostratus, altocumulus and altostratus (purple-coloured triangles).

As a conclusion, the test applied to SEVIRI should be modified as follows:

- The thresholds applied to R1.6µm should be modified to increase its value and to improve the dependency with viewing angles. Figure 8.1.8 shows such an improved threshold, computed as explained in Ref[1], but assuming snow particle's size of 250 and 70 micron instead only 250 micron.
- The threshold applied to T3.9µm -T10.8µm should be decreased to account for the shape of the 3.9µm channel spectral filter beyond the 4 micron.
- T3.9µm -T10.8µm should be used **together** with R1.6µm to reduce the misclassification of thin cirrus. In that case, the test applied to T10.8µm -T12.0µm could be removed.

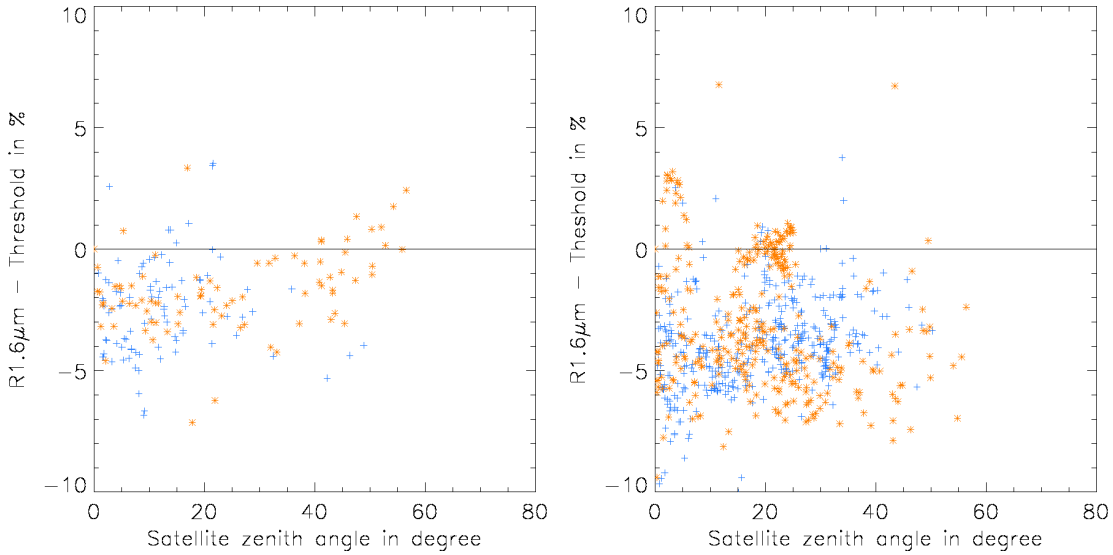

Figure 8.1.8 Variation of R1.6µm reflectance minus the improved threshold with satellite zenith angles for solar zenith angles lower (left) or higher (right) than 50 degrees. In the forward scatter (brown *) or backward scatter (blue +) direction.

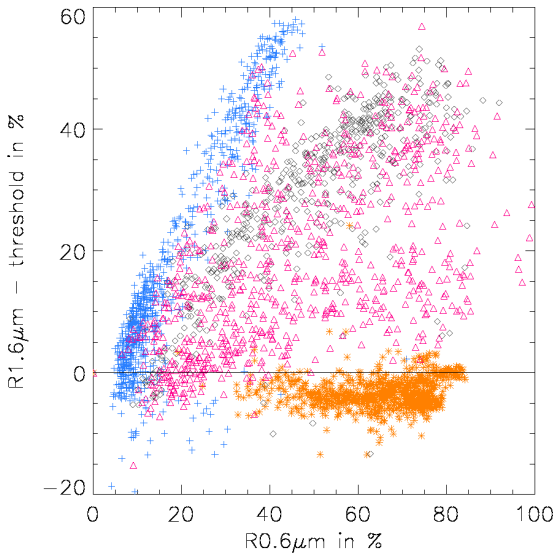

Figure 8.1.9 Variation of R1.6µm reflectance minus the improved thresholds with R0.6µm visible reflectance for cloud free continental surface (blue +), snow (brown *), stratus, stratocumulus or cumulus clouds (black diamond), cirrus (over land or low clouds), cirrostratus, altocumulus and altostratus (purple-coloured triangles).

8.2 SNOW AT NIGHT-TIME

The three following figures give an insight of the snow infrared properties in nighttime conditions, as seen by MODIS. It seems as if snow could be distinguished from cloud free continental surfaces or low clouds by their higher T8.7µm-T10.8µm (figure 8.2.1) and lower T10.8µm-T3.9µm (figure 8.2.2) values. Nevertheless, it will be very difficult to automatically perform this separation because:

- The differences are rather low (around one degree)

- The comparison of figures 8.2.1 and 8.1.7 shows that a diurnal effect exists in the T8.7µm-T10.8µm values for snow, making the use of this feature dependent on the time of the day.

On the other hand, the separation of snow from thin ice clouds does not seem possible.

No algorithm are yet proposed.

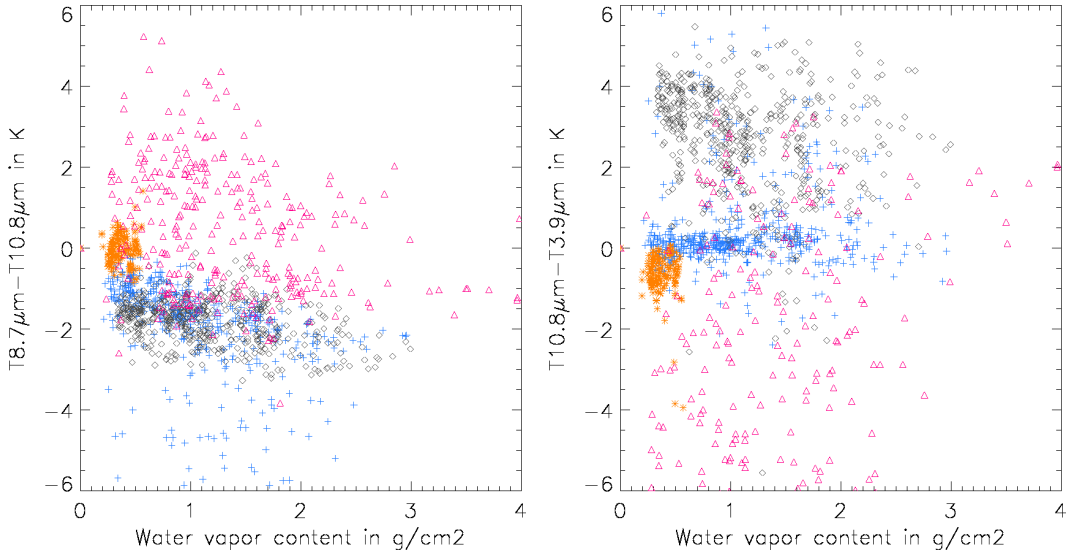

Figure 8.2.1 Variation of nighttime T8.7µm-T10.8µm (left) or T10.8µm-T3.9µm (right) brightness temperature difference with integrated atmospheric water vapour for cloud free continental surface (blue +), snow (brown *), stratus, stratocumulus or cumulus clouds (black diamond), cirrus (over land or low clouds), cirrostratus, altocumulus and altostratus (purple-coloured triangles).

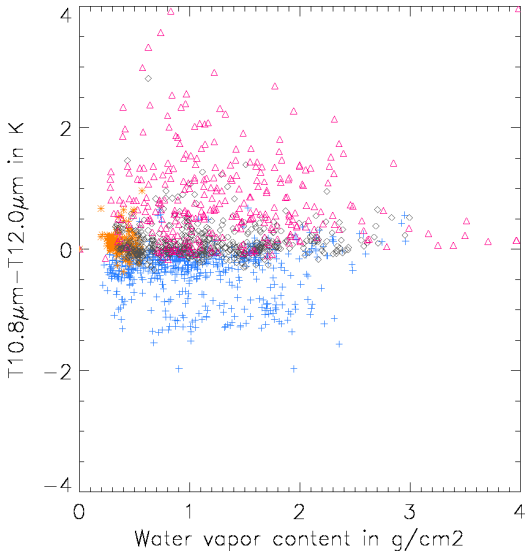

Figure 8.2.2 Variation of nighttime T10.8µm-T12.0µm (right) brightness temperature difference with integrated atmospheric water vapour for cloud free continental surface (blue +), snow (brown *), stratus, stratocumulus or cumulus clouds (black diamond), cirrus (over land or low clouds), cirrostratus, altocumulus and altostratus (purple-coloured triangles).

9. IDENTIFICATION OF VOLCANIC ASH CLOUDS

The identification of volcanic ash clouds includes their separation from cloud free areas (ocean or land) as well as from water or ice clouds, and from dust clouds.

This study analyses the spectral behaviour of cloud free areas, water/ice/dust clouds and volcanic ash clouds from the MODIS interactive targets. The following volcanic events have been analysed using MODIS imagery:

- Shevelush (Kamchatka Peninsula, Russia) : 28th-29th August 2000 (72 targets), 19th May 2001 (48 targets),
- Cleveland (Aleutian Islands, USA) : 19th-20th February 2001 (99 targets), 11th-12th march 2001 (119 targets)
- Etna (Italy): 20th-21st-22nd-24th July 2001 (524 targets)

Results obtained in a previous study using GOES imagery (Ref.[1]) are also included in this study because they are in contradiction with those obtained with MODIS. This previous study focuses on two volcanoes in tropical areas: La Souffriere, West Indies (18th September 1996, 8th August 1997, 14th December 1998, 13th January 1999, 10th May 1999) and Popocatepelt, Mexico (12th March 1996).

We refer in the following paragraphs to information delivered during a international workshop dedicated to the remote sensing of volcanic clouds which was held in Michigan technical University on end July 2001.

9.1 THE USE OF T10.8µM-T12.0µM

The most classical spectral feature used in volcanic ash clouds detection is the T10.8µm-T12.0µm brightness temperature difference. Volcanic ash clouds are detected by their negative T10.8µm-T12.0µm values. Limitations of this method are known: volcanic ash clouds may exhibit positive differences when containing ice or when observed with moist atmosphere that may "hide" the ash effect.

Figures 9.1.1 and 9.1.2 illustrates the skill of this feature to separate volcanic ash clouds from cloud free areas and water/ice/dust clouds in MODIS and GOES imagery. T10.8µm-T12.0µm brightness temperature difference seems very successful to characterize volcanic ash clouds in MODIS imagery, which is confirmed by a visualization of the images. Nevertheless, the following limitations of the method are illustrated in figures 9.1.1 and 9.1.2:

- most volcanic ash clouds present positive T10.8µm-T12.0µm values (up to 6ºC) in GOES imagery, in contradiction with was is observed in MODIS imagery. Note that the two volcanoes analysed in GOES imagery are located in tropical areas.
- clouds (essentially cumulus and cumulonimbus clouds) may have highly negative T10.8µm-T12.0µm values (-1ºC, -2ºC) in GOES imagery. This is not observed in MODIS imagery.
- Cloud free continental areas may have highly negative T10.8µm-T12.0µm values (-2ºC, -3ºC) in non-vegetated areas.
- T10.8µm-T12.0µm does not allow the discrimination of volcanic ash clouds from dust clouds.

In spite of all the drawbacks quoted above, T10.8µm-T12.0µm has proved really efficient for the visualization of most volcanic ash clouds that we have studied with MODIS imagery (even volcanic ash clouds above lower clouds could be visually identified). This is why we will develop a volcanic ash cloud detection algorithm based on this feature and using additional channels to minimise the false alerts ratio. The major problem is that this algorithm will not detect eruptions

characterized by highly positive T10.8µm-T12.0µm. The following paragraphs analyse the potential contribution of other channels to minimise the false alarm ration.

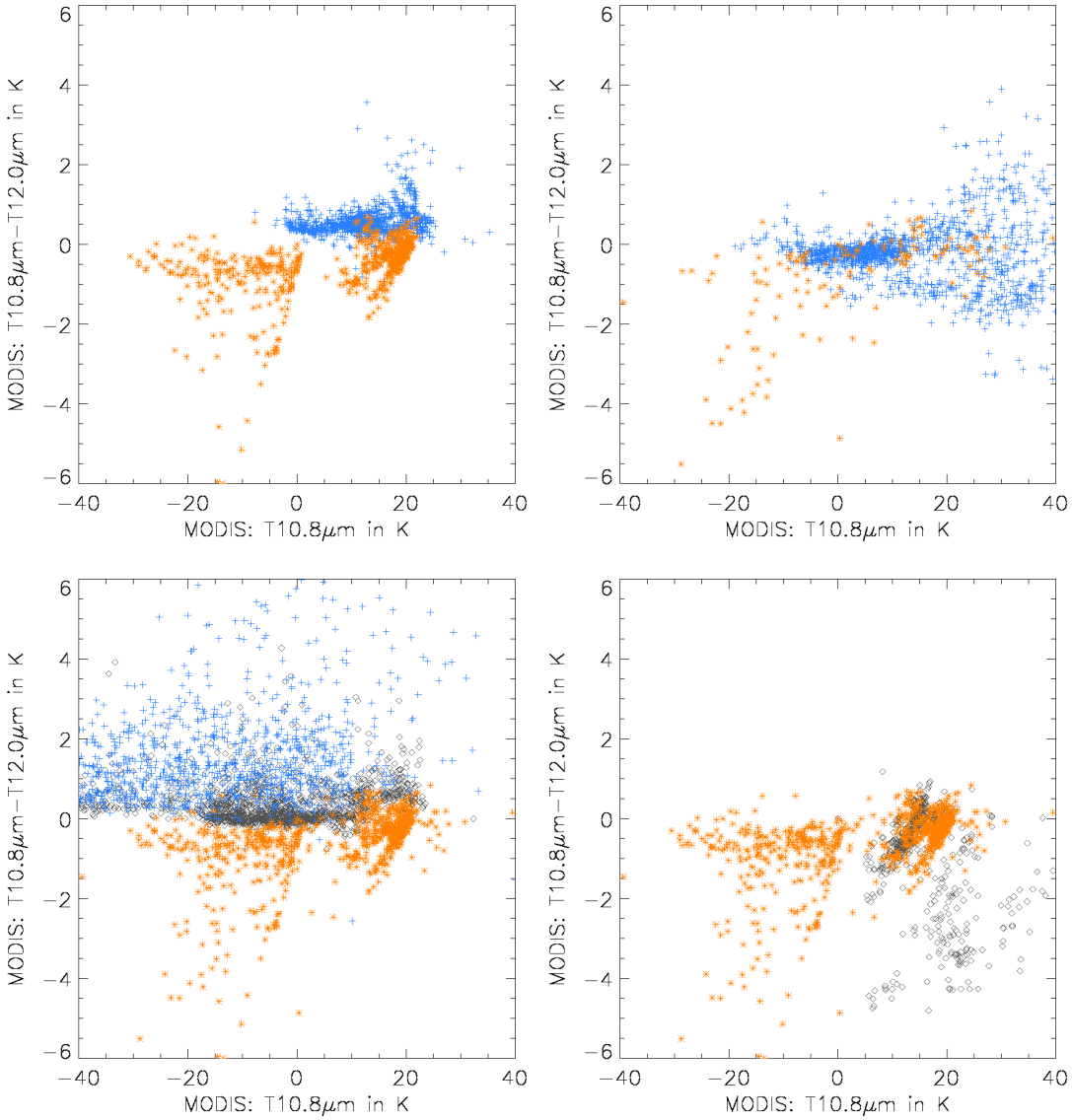

Figure 9.1.1 Variation of MODIS T10.8µm-T12.0µm brightness temperature difference with T10.8µm.
Top left: cloud free oceanic surface (blue +) and volcanic ash clouds over sea (brown *)
Top right: cloud free continental surface (blue +) and volcanic ash clouds over land (brown *)
Bottom left: volcanic ash clouds (brown *), stratus, stratocumulus, cumulus and cumulonimbus clouds, altocumulus and altostratus (black diamond), Cirrus, cirrostratus, (blue +)
Bottom right: volcanic ash clouds (brown *), dust clouds (black diamond)

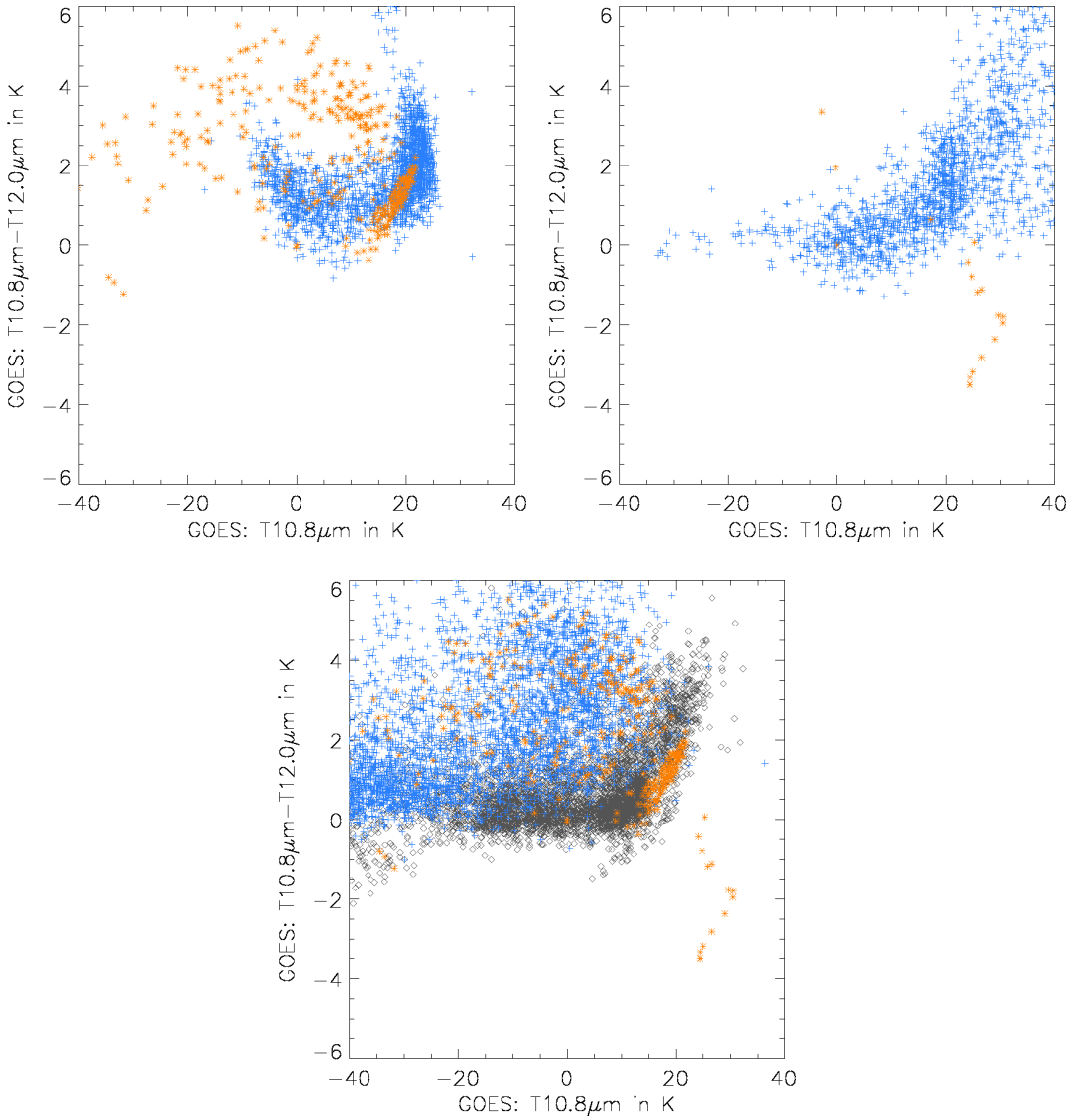

Figure 9.1.2 Variation of GOES T10.8µm-T12.0µm brightness temperature difference with T10.8µm.
Top left: cloud free oceanic surface (blue +) and volcanic ash clouds over sea (brown *)
Top right: cloud free continental surface (blue +) and volcanic ash clouds over land (brown *)
Bottom: volcanic ash clouds (brown *), stratus, stratocumulus, cumulus and cumulonimbus clouds, altocumulus and altostratus (black diamond), Cirrus, cirrostratus, (blue +)

9.2 THE USE OF T3.9µM-T10.8µM

The T3.9µm-T10.8µm brightness temperature differences have been recently used, together with T10.8µm-T12.0µm, to detect volcanic ash clouds: volcanic ash clouds are characterized at daytime by high reflectance at 3.9µm, leading to high T3.9µm-T10.8µm values.

Figures 9.2.1 - 9.2.4 illustrates the skill of this feature to separate volcanic ash clouds from cloud free areas and water/ice/dust clouds in MODIS and GOES imagery.

It is interesting to notice that at nightime, T3.9µm-T10.8µm should allow an efficient separation of volcanic ash clouds from cloud free area, low clouds or dust clouds (certainly due, as for cirrus clouds, to the volcanic ash semi-transparency and the non linearity effect in Planck function).

At daytime, volcanic ash clouds T3.9µm-T10.8µm values are not very different from that of water, ice or dust clouds, but are usually higher than cloud free's values.

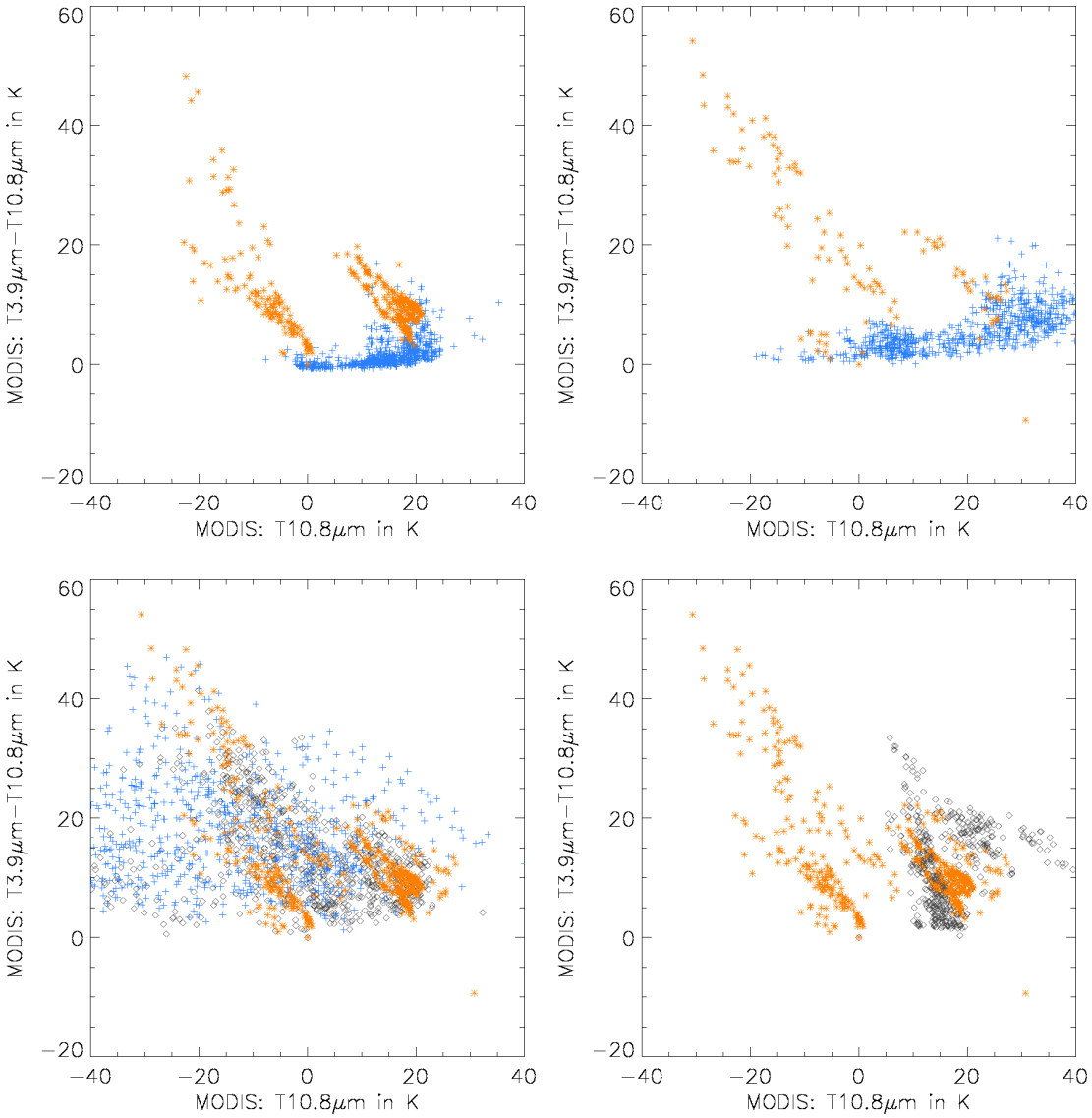

Figure 9.2.1 Daytime MODIS T3.9µm-T10.8µm brightness temperature difference.
Top left: cloud free oceanic surface (blue +) and volcanic ash clouds over sea (brown *)
Top right: cloud free continental surface (blue +) and volcanic ash clouds over land (brown *)
Bottom left: volcanic ash clouds (brown *), stratus, stratocumulus, cumulus and cumulonimbus clouds, altocumulus and altostratus (black diamond), Cirrus, cirrostratus, (blue +)
Bottom right: volcanic ash clouds (brown *), dust clouds (black diamond)

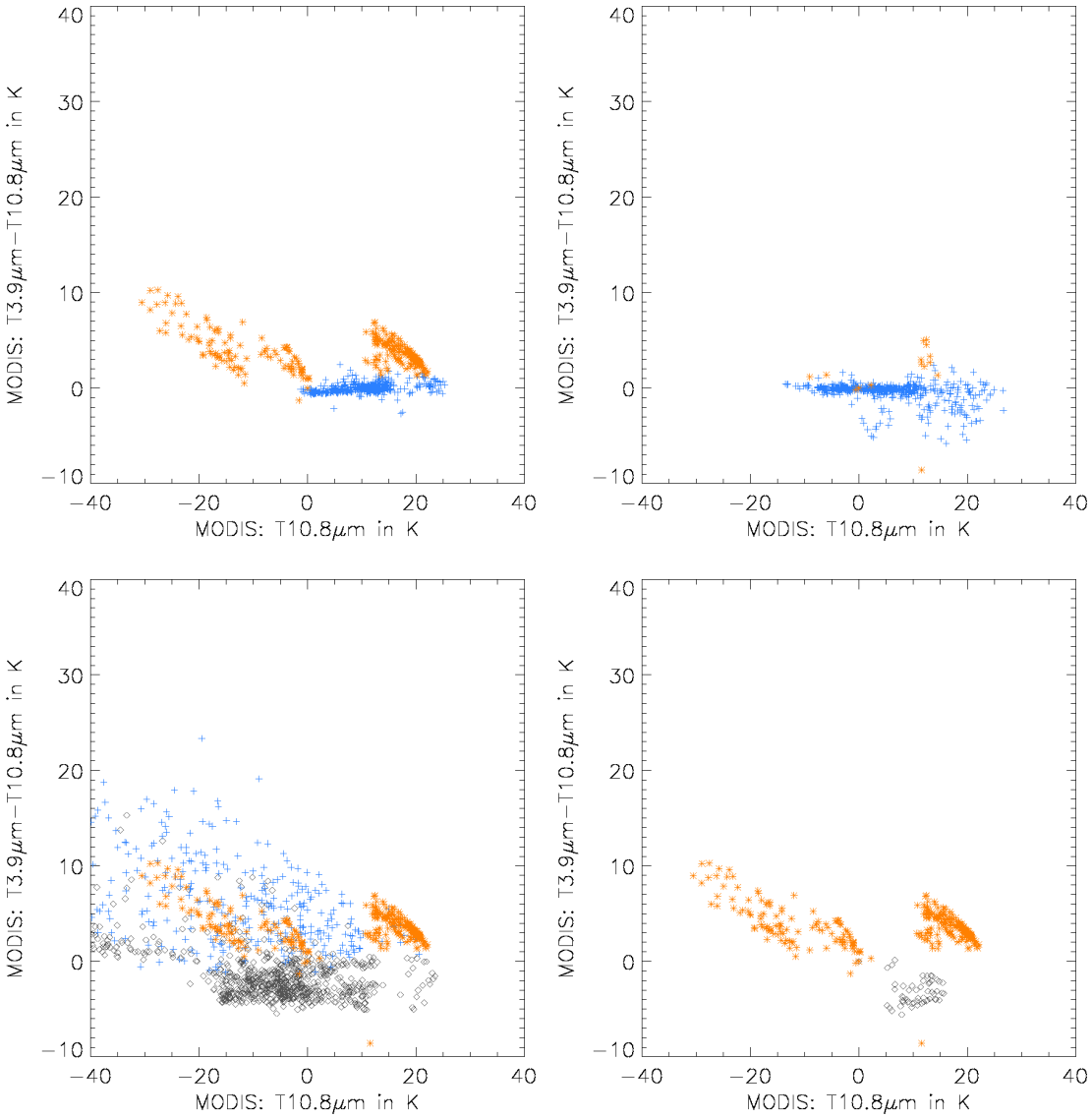

Figure 9.2.2 Nighttime MODIS T3.9µm-T10.8µm brightness temperature difference.
Top left: cloud free oceanic surface (blue +) and volcanic ash clouds over sea (brown *)
Top right: cloud free continental surface (blue +) and volcanic ash clouds over land (brown *)
Bottom left: volcanic ash clouds (brown *), stratus, stratocumulus, cumulus and cumulonimbus clouds, altocumulus and altostratus (black diamond), Cirrus, cirrostratus, (blue +)
Bottom right: volcanic ash clouds (brown *), dust clouds (black diamond)

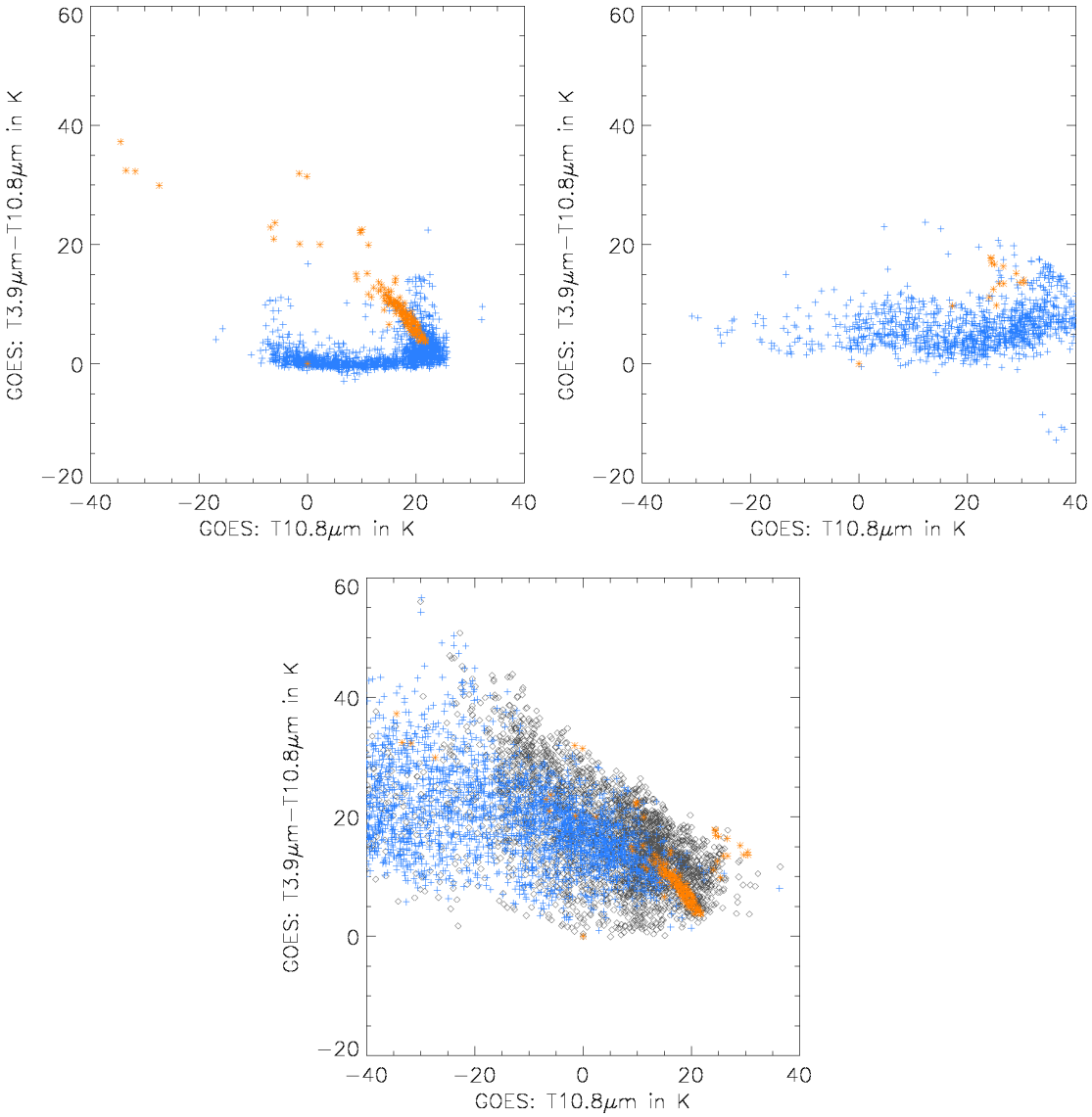

Figure 9.2.3 Daytime GOES T3.9µm-T10.8 µm brightness temperature difference.
Top left: cloud free oceanic surface (blue +) and volcanic ash clouds over sea (brown *)
Top right: cloud free continental surface (blue +) and volcanic ash clouds over land (brown *)
Bottom: volcanic ash clouds (brown *), stratus, stratocumulus, cumulus and cumulonimbus clouds, altocumulus and altostratus (black diamond), Cirrus, cirrostratus, (blue +)

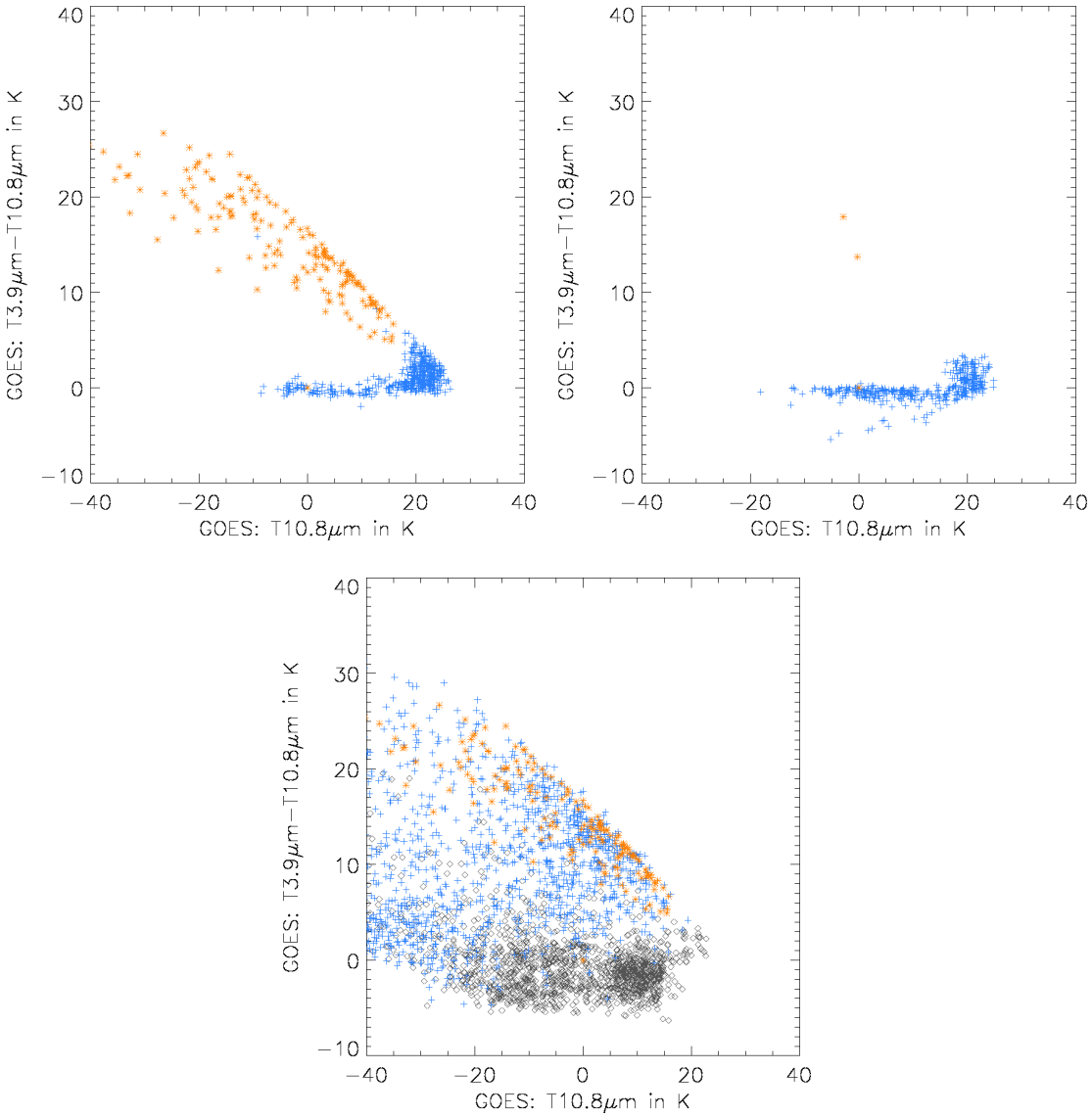

Figure 9.2.4 Nighttime GOES T3.9µm-T10.8µm brightness temperature difference.
Top left: cloud free oceanic surface (blue +) and volcanic ash clouds over sea (brown *)
Top right: cloud free continental surface (blue +) and volcanic ash clouds over land (brown *)
Bottom: volcanic ash clouds (brown *), stratus, stratocumulus, cumulus and cumulonimbus clouds, altocumulus and altostratus (black diamond), Cirrus, cirrostratus, (blue +)

9.3 THE USE OF T8.7µM

This new channel at 8.7µm is supposed to be sensitive to sulphuric aerosol absorption, but also to silicate ash. Volcanic ash clouds should therefore be characterized by highly negative T8.7µm-T10.8µm or T8.7µm-T12.0µm brightness temperature differences.

Figures 9.3.1 illustrates the skill of T8.7µm-T10.8µm brightness temperature difference to separate volcanic ash clouds from cloud free areas and water/ice/dust clouds. These figures are not so encouraging. When visualizing images to better understand these results, it can be seen that:

- Volcanic ash from the Etna clearly induces an increase of T8.7µm-T10.8µm (corresponds to the warmest targets in figure 9.3.1)
- Volcanic ash from the Shevelush and the Cleveland usually induces a decrease of T8.7µm-T10.8µm which may be strong (less than –5ºC; corresponds to the targets with T10.8µm brightness temperatures between 0ºC and –10ºC). The positive T8.7µm-

T10.8µm values (with T10.8µm brightness temperatures lower than –10ºC) corresponds to thin volcanic ash overlaying other clouds: in that case the volcanic ash T8.7µm-T10.8µm signature is masked by that of the underlying cloud (see for example figure 7.3). Note that in that case, the volcanic ash can still be visualized by its lower T10.8µm-T12.0µm.

An additional difficulty is the highly negative T8.7µm-T10.8µm values over desertic areas which could be misclassified as volcanic ash clouds. Finally T8.7µm-T10.8µm does not allow the distinction between volcanic ash and dust clouds.

In spite of all these drawbacks, the T8.7µm-T10.8µm feature could be used in complement with the T10.8µm-T12.0µm feature, except over arid areas.

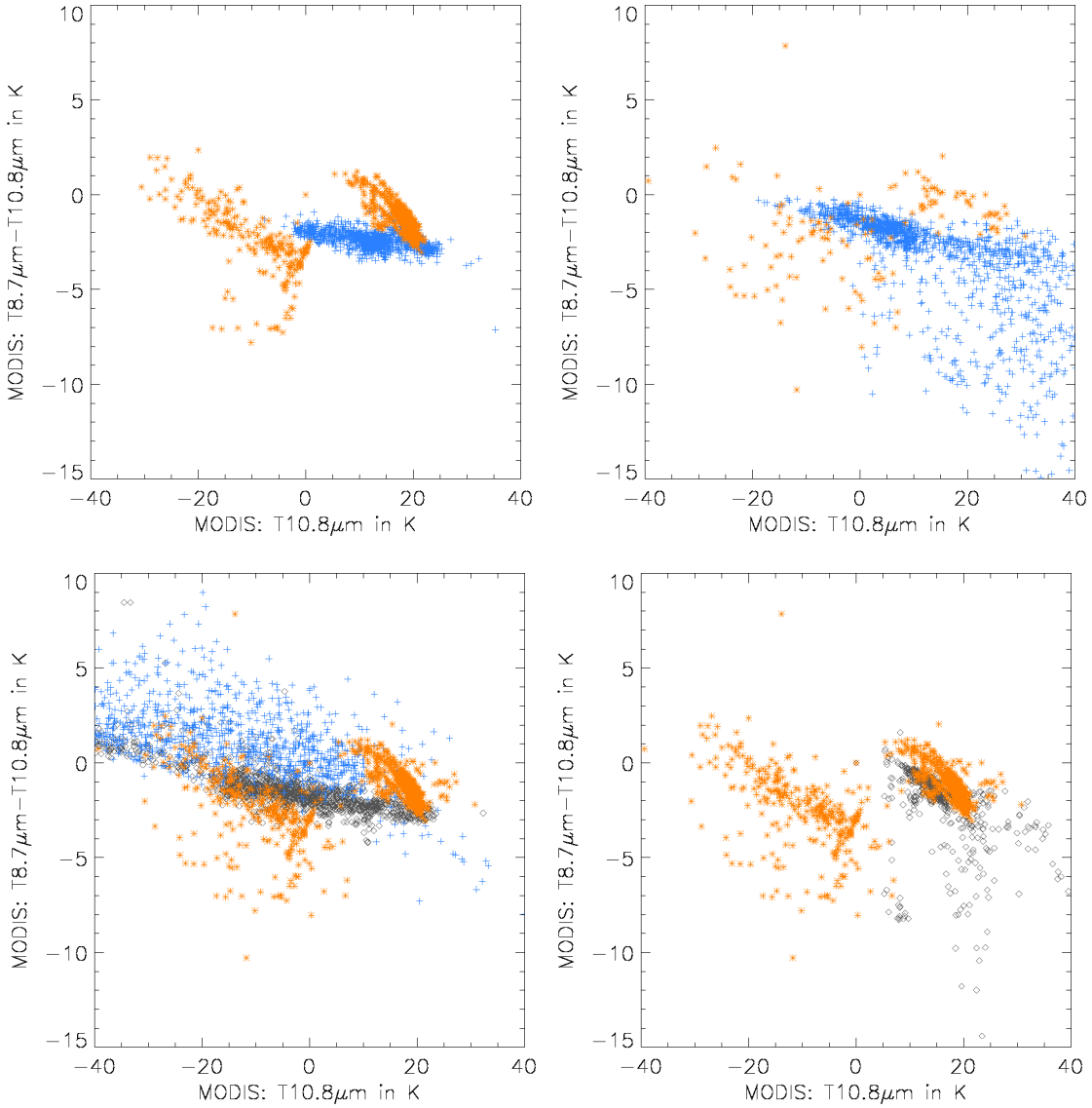

Figure 9.3.1 Variation of MODIS T8.7µm-T10.8µm brightness temperature difference with T10.8µm.
Top left: cloud free oceanic surface (blue +) and volcanic ash clouds over sea (brown *)
Top right: cloud free continental surface (blue +) and volcanic ash clouds over land (brown *)
Bottom left: volcanic ash clouds (brown *), stratus, stratocumulus, cumulus and cumulonimbus clouds, altocumulus and altostratus (black diamond), Cirrus, cirrostratus, (blue +)
Bottom right: volcanic ash clouds (brown *), dust clouds (black diamond)

9.4 THE USE OF 1.6µM

The volcanic ash clouds are supposed to be characterized by higher reflectance at 1.6µm than at 0.6µm which is not the case for water or ice clouds. This property should help in the volcanic ash cloud identification.

Figures 9.4.1 illustrates the skill of R1.6µm reflectance difference to separate volcanic ash clouds from cloud free areas and water/ice/dust clouds. This is not in agreement with what was expected.

It can be observed that reflectances of volcanic ash clouds at 0.6 and 1.6µm are rather close together, which is not the case for desertic areas and not systematic for clouds.

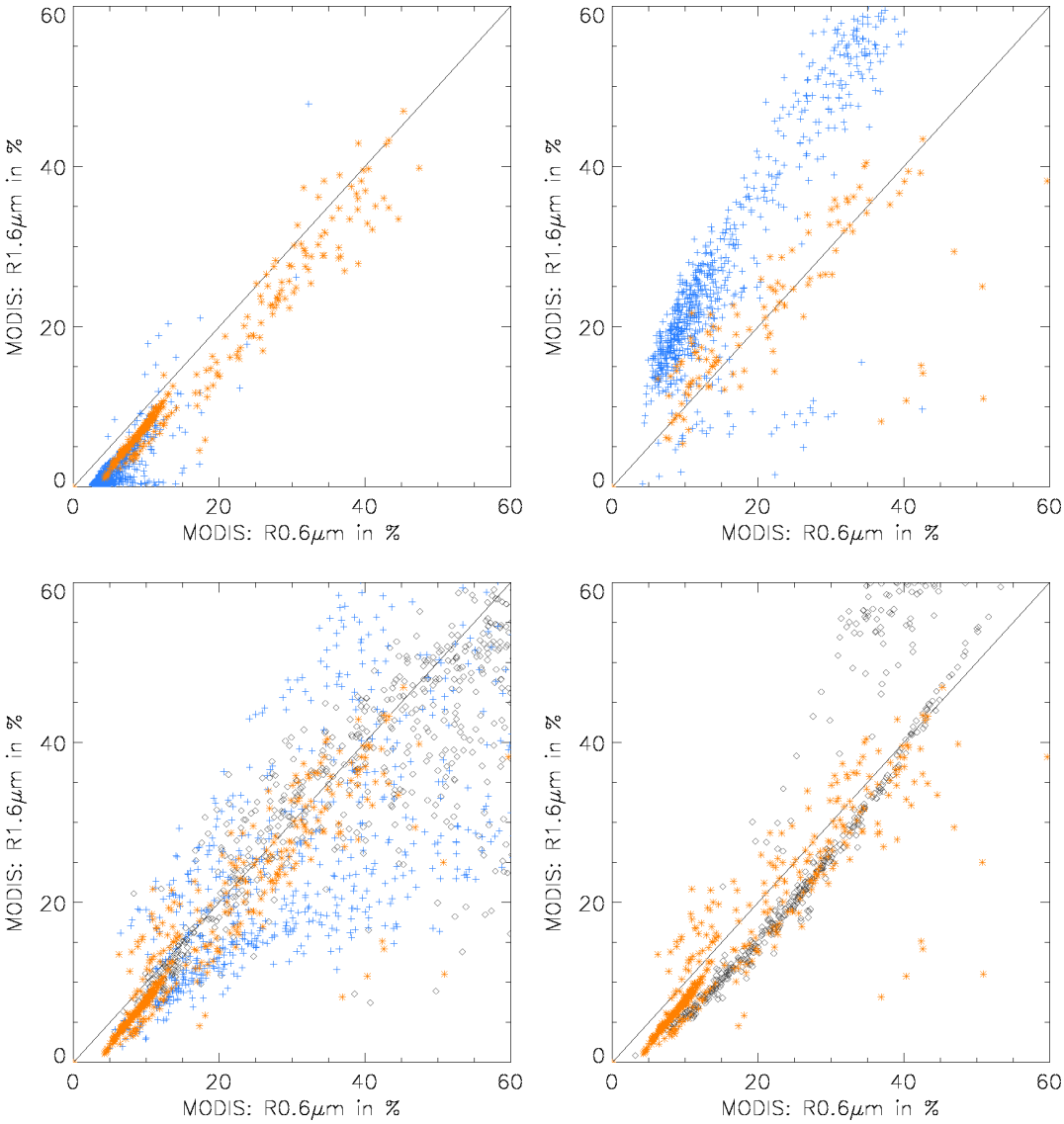

Figure 9.4.1 Variation of MODIS R1.6µm reflectance with R0.6µm visible reflectance.
Top left: cloud free oceanic surface (blue +) and volcanic ash clouds over sea (brown *)
Top right: cloud free continental surface (blue +) and volcanic ash clouds over land (brown *)
Bottom left: volcanic ash clouds (brown *), stratus, stratocumulus, cumulus and cumulonimbus clouds, altocumulus and altostratus (black diamond), Cirrus, cirrostratus, (blue +)
Bottom right: volcanic ash clouds (brown *), dust clouds (black diamond)

9.5 THE USE OF 9.7, 7.3µM FOR SO_2 DETECTION

Channels at 9.7 and 7.3 micrometer are sensitive to SO_2 absorption. Results of the use of these channels (in combination with channels at 12.0 or 13.4 micrometer) for volcanic ash cloud identification in the Cleveland eruption of 19th February 2001 have been presented during the international workshop held in Michigan, USA in July 2001.

Next figures 9.5.1, 9.5.2 and 9.5.3 illustrate the skill of these channels in the characterisation of volcanic ash clouds. T7.3µm-T12.0µm and T9.7µm-T12.0µm values (for a given T10.8µm) are lower for volcanic ash clouds than for water or ice clouds values (thus indicating a stronger absorption) only in the case of the Cleveland volcano. This not at all the case for the Etna eruption. Anyhow, it will be difficult to automatize the use of these features.

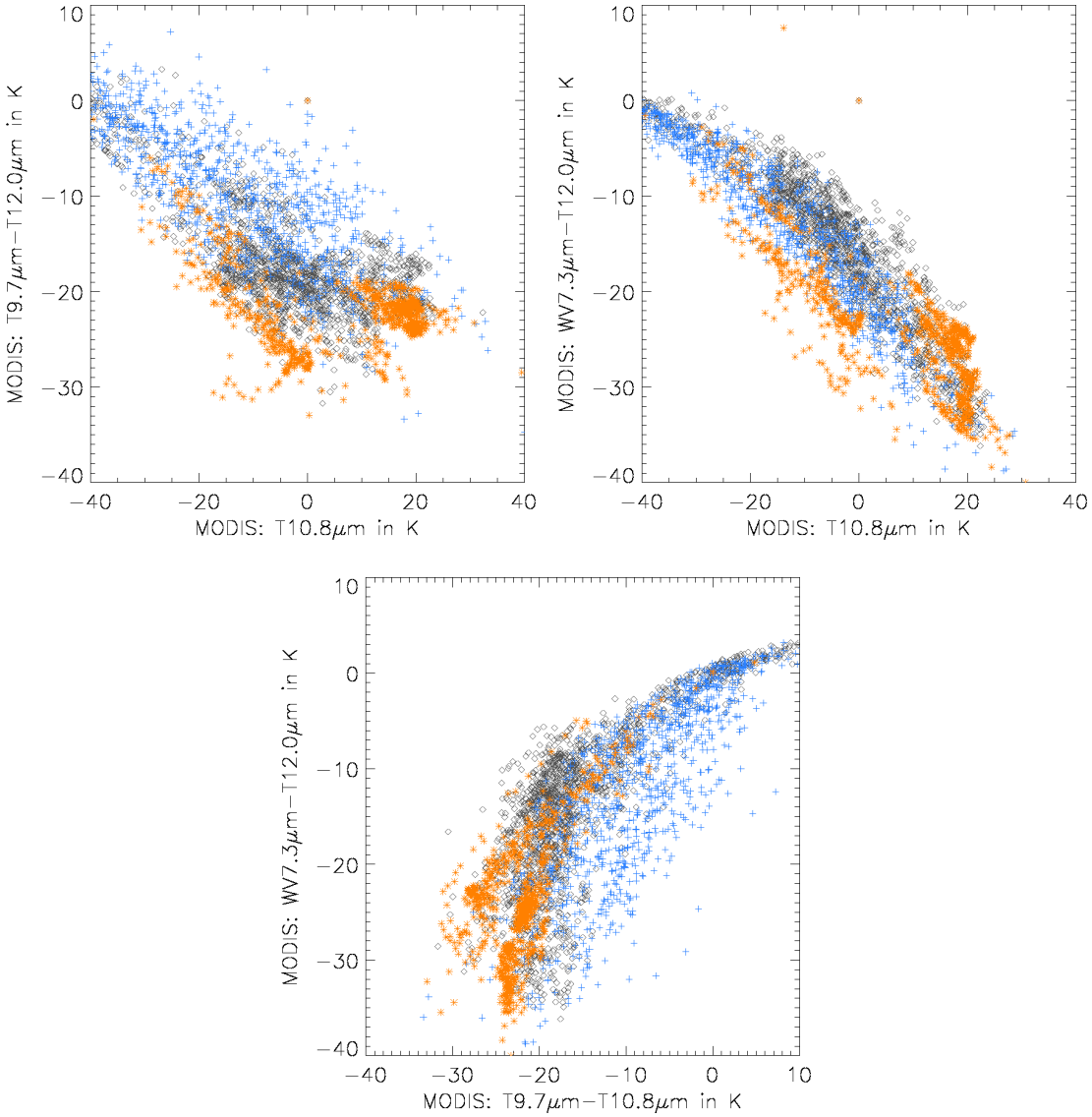

Figure 9.5.1 Illustration of MODIS T9.7µm and WV6.7µm impact on volcanic ash cloud characterization. Volcanic ash clouds (brown *), stratus, stratocumulus, cumulus and cumulonimbus clouds, altocumulus and altostratus (black diamond), Cirrus, cirrostratus, (blue +)

9.6 VOLCANIC ASH CLOUD DETECTION WITH SEVIRI

The method described in this paragraph will be tested on MODIS imagery before being implemented in the SEVIRI processing scheme. This method will only provide a flag which will

indicates the presence of volcanic ash clouds [except those characterised by high positive T10.8µm-T12.0µm (in moist atmosphere or containing ice…)], but will also include false alarms.

At nightime or twilight, a pixel is classified as contaminated by volcanic ash if:

- T12.0µm -T10.8µm > thresholdT120T108 or T10.8µm –T8.7µm > thresholdT108T87 (except in arid areas)
- T3.9µm -T10.8µm > thresholdT39T108

[thresholdT120T108, thresholdT108T87 and thresholdT39T108 should depend on atmospheric water vapour content and viewing angles (could be pre-computed using RTTOV cloud free simulation)]

At daytime, a pixel is classified as contaminated by volcanic ash if:

- T12.0µm -T10.8µm > thresholdT120T108 or T10.8µm –T8.7µm > thresholdT108T87 (except in arid areas)
- T3.9µm -T10.8µm > thresholdT39T108
- |R0.6-R1.6| < thresholdR06R16
- R0.6 > thresholdR06 (only over ocean outside sunglint area)

[thresholdT120T108, thresholdT108T87 and thresholdT39T108 should depend on atmospheric water vapour content and viewing angles (could be pre-computed using RTTOV cloud free simulation); thresholdR06 should be similar to the one used in cloud detection (but with a lower offset); thresholdR06R16 will be an empirical value (10%)]

10. IDENTIFICATION OF DUST CLOUDS

During the development, the following algorithm to detect dust events was designed using AVHRR and GOES imagery (see Ref [1]):

Over the ocean at daytime, a pixel is classified as contaminated by dust if:

- R06threshold < R0.6µm < R06threshold + 30%
- -5°C –5*(1/cos(θsat)-1) < T11µm – SSTclim
- SD(10.8µm) < 0.4°C and SD(0.6µm) < 0.6%

Over continental surfaces at daytime, a pixel is classified as contaminated by dust if:

- 0°C < T10.8µm < 37°C and (T3.9µm – T10.8µm) / cos(θsol) > 30°C
- R06threshold –15% < R0.6µm < R06threshold + 30%
- SD(10.8µm) < 0.4°C and SD(0.6µm) < 0.6%

[R06threshold is a threshold used in the cloud detection process, SD is the standard deviation, θsat and θsol are the satellite and solar zenith angles, SSTclim is the climatological Sea Surface Temperature].

MODIS imagery is used to check and improve this algorithm, for its final application to SEVIRI.

13 Dust events have been selected, and corresponding MODIS imagery desarchived:

Date	location	Time of the day
19th August 2000	Sahara	Day & night
26th September 2000	West African coast	Day & night
8th February 2001	North African coast	Day & night
10th February 2001	West African coast	Day only
11th February 2001	West African coast	Day & night
12th February 2001	West African coast	Day only
13th February 2001	West African coast	Day only
15th February 2001	West African coast	Day only
16th April 2001	Sahara	Day & night
17th April 2001	North African coast	Day & night
18th April 2001	North African coast	Day & night
21st April 2001	North African coast	Day only
25th April 2001	Sahara	Day & night

MODIS images have been visualized, in order to get a first insight into the usefulness of the several spectral bands. Interactive targets corresponding to dust events have been manually gathered from the 13 selected dust events [mostly in daytime imagery (185 over land, 430 over sea) and only very few at nighttime (22 over land and 38 over sea)], to allow a more quantitative analysis of the dust identification.

10.1 OVER THE OCEANS:

Over the ocean, dust events are easily identified by their high smooth reflectance (either at 0.6, 0.8 or 1.6µm), but this can be performed only at daytime outside sunglint areas. Visual identification of dust events is rather difficult at nighttime. This is by the way the reason why so few dust targets have been extracted from nighttime images: to ease the visual identification during this study, daytime and nighttime images from the same day over the same area have been simultaneously analysed.

It has been observed that dust is also usually characterized by lower T10.8µm-T12.0µm and higher T8.7µm-T10.8µm than oceanic cloud free surfaces. But situations may be found, where this is not the case: on 21th April over North African Coast, a dust outbreak from Lybia presents rather high T10.8µm-T12.0µm values, maybe because the dust is just coming from the desert and is still warmer than the ocean. Nighttime dust signature in T10.8µm-T3.9µm is more

"incoherent": we found one case (17th April) where highly positive values (larger that cloud free oceanic values) have been found, whereas usually negative values (lower than oceanic values) are observed. At daytime, T10.8µm-T3.9µm is usually lower than cloud free oceanic values.

If dust can easily be separated from ice clouds by their high T10.8µm-T12.0µm, the confusion with low clouds seems to be solved by their slightly lower T10.8µm-T12.0µm or larger T8.7µm-T10.8µm.

These features can be quantified, using the interactive targets (only daytime, too few targets in nightime conditions):

- The reflectances (either at 0.6, 0.8 or 1.6µm) are very efficient to detect dust at daytime (except in sunglint areas), as shown on figure 10.1.1. But these reflectances do not allow a clear separation with low clouds.

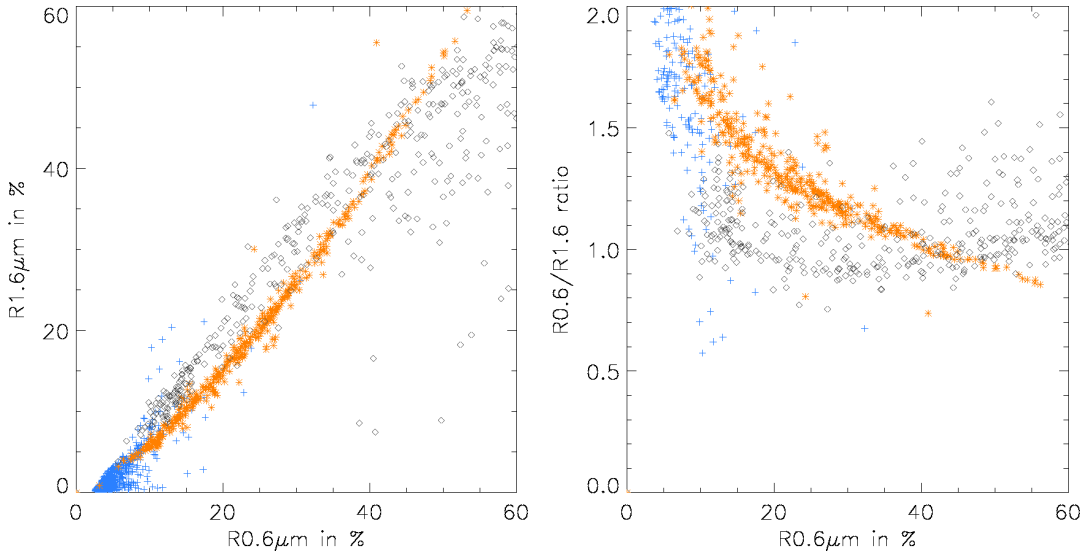

Figure 10.1.1 Variation of R1.6µm reflectance (left) and R0.6µm/ R1.6µm reflectance ratio (right) with R0.6µm reflectance. For oceanic cloud free surface (blue +), low clouds (black diamond) and dust (brown *)

- T10.8µm-T12.0µm decreases with dust's thickness, whereas T8.7µm-T10.8µm increases, as shown on figure 10.1.2. The rate of the observed increase (or decrease) depends on the situation (larger variation on 8th February than on 18th April, both on West African coast), as shown on figure 10.1.3. This behaviour is in apparent contradiction with simulations presented in Ackerman, 1997. These features should be efficient to separate in most cases dust events from sea surface when reflectance cannot be used (at nighttime or in sunglint). Moreover, T10.8µm-T12.0µm allows the separation with ice clouds, and even with low clouds (as indicated by figure 10.1.1). These brightness temperatures' differences for oceanic cloud-free surfaces depends on atmospheric water vapour content (as shown on figure 10.2.4), but also on scanning angle: a similar approach to the computation of the thresholds used in the cloud detection tests is required to develop an efficient dust detection scheme.

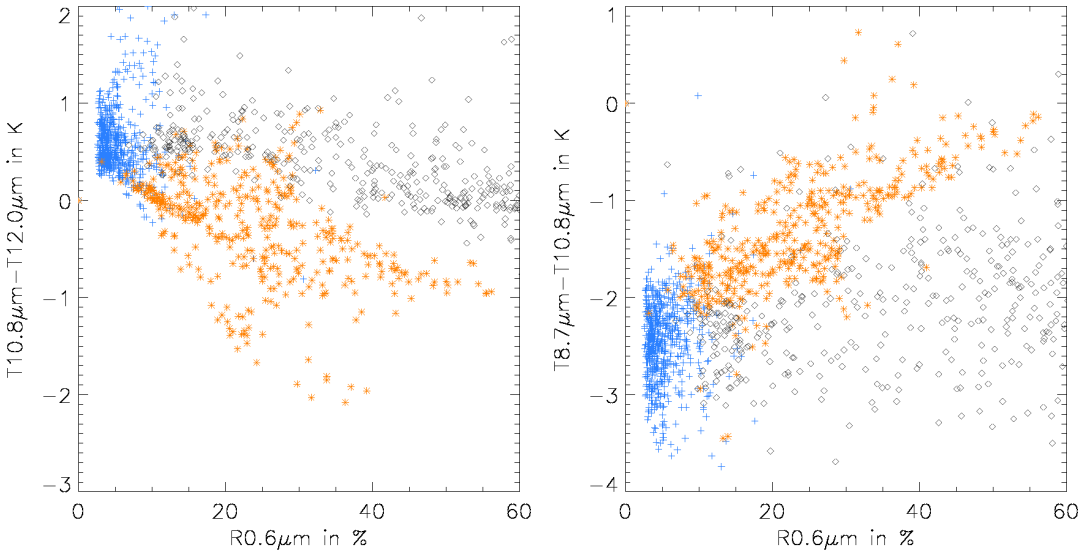

Figure 10.1.2 Variation of T10.8µm-T12.0µm and T8.7µm-T10.8µm brightness temperature differences with R0.6µm reflectance. For oceanic cloud free surface (blue +), low clouds (black diamond) and dust (brown *)

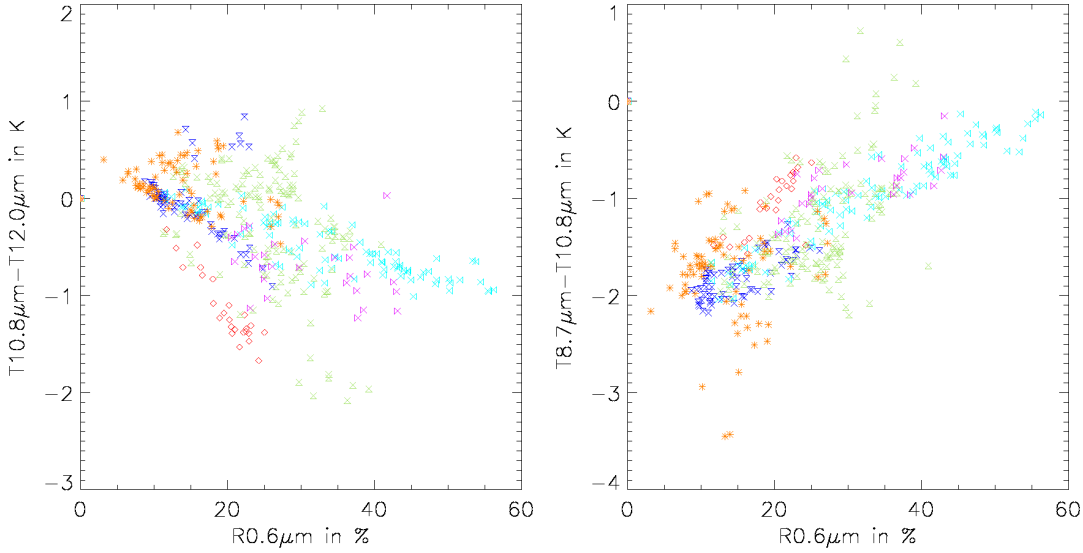

Figure 10.1.3 Variation of T10.8µm-T12.0µm and T8.7µm-T10.8µm brightness temperature differences with visible reflectance for dust events: 8th February (red), 13th February (dark blue), 17th April (purple), 18th April (light blue), 21th April (pale green), other days: brown.

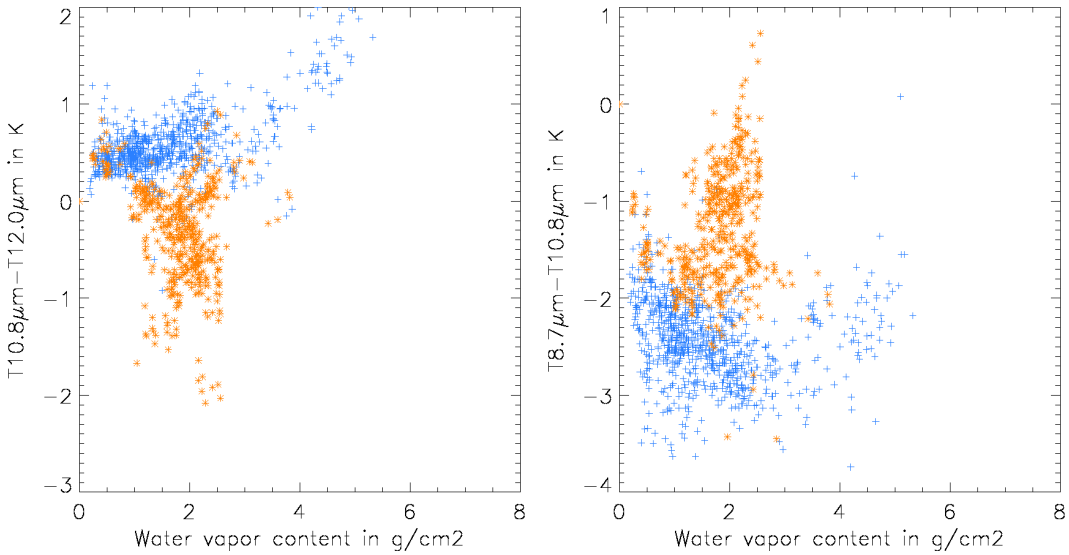

Figure 10.1.4 Variation of T10.8µm-T12.0µm and T8.7µm-T10.8µm brightness temperature differences with water vapour content. For oceanic cloud free surface (blue +), dust (brown *).

- During daytime, T3.9µm-T10.8µm increases with dust's thickness [in accordance with simulations presented in Ackerman, 1997], but at a lower rate than observed with AVHRR (see Ref[1]). This feature seems less efficient than T10.8µm-T12.0µm for dust's separation with cloud free oceanic surface. Moreover, this feature does not allow a distinction with low clouds.

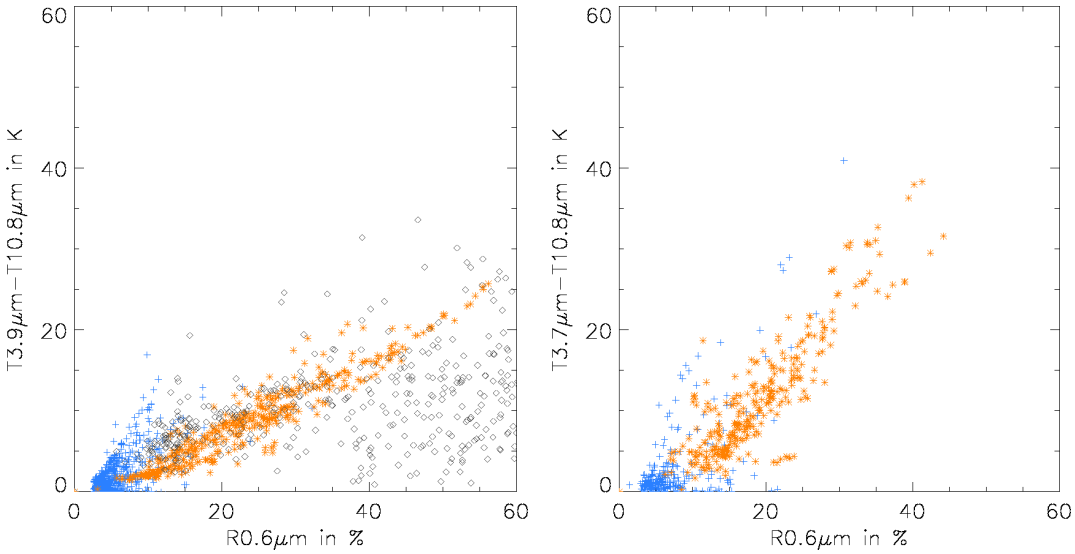

Figure 10.1.5 Variation of T3.9µm-T0.8.0µm (T3.7µm-T0.8.0µm for AVHRR) brightness temperature difference with visible reflectance for MODIS targets (left) and AVHRR targets (right). Oceanic cloud free surface (blue +), dust (brown *) and low clouds (black diamond).

As a conclusion, the 1.6µm channel will not be used to improve the dust identification over oceanic areas. Instead, T8.7µm-T10.8µm and T10.8µm-T12.0µm will be included in an updated algorithm that will be tested before being implemented in the SEVIRI scheme:

Over the ocean at daytime (outside sunglint), a pixel is classified as contaminated by dust if:

- R06threshold < R0.6µm < R06threshold + 30%
- -5°C –5*(1/cos(θsat)-1) < T11µm – SSTclim
- T10.8µm -T12.0µm < T108T120threshold-3°C [TBD]
- T8.7µm -T10.8µm > T87T108threshold
- SD(10.8µm) < 0.4°C and SD(0.6µm) < 0.6%

Over the ocean at nighttime, in twilight conditions or in sunglint area, a pixel is classified as contaminated by dust if:

- -5°C –5*(1/cos(θsat)-1) < T11µm – SSTclim
- T10.8µm -T12.0µm < T108T120threshold-3°C [TBD]
- T8.7µm -T10.8µm > T87T108threshold
- SD(10.8µm) < 0.4°C

[R06threshold, T108T120threshold and T87T108threshold are thresholds used in the cloud detection process, SD is the standard deviation, θsat is the satellite zenith angles, SSTclim is the climatological Sea Surface Temperature].

10.2 OVER THE CONTINENTAL AREAS:

The visual identification of dust events is much more difficult over land than over sea, because the continental surfaces are brighter than the ocean, thus reducing the contrast of dust in the solar channels (either at 0.6, 0.8 or 1.6µm). Dust may be detected at daytime by using the thermal contrast between dust and overheated surfaces; this technique is hardly applicable at nighttime. To ease the visual identification during this study, daytime and nighttime images from the same day over the same area have been simultaneously analysed. But the visual identification of dust at nighttime remains very difficult, and consequently very few targets were extracted.

The contribution of spectral bands to dust detection has been visually analysed, and quantified when possible, but only at daytime:

- Dust can hardly be visually detected with R1.6µm over bright grounds, as confirmed on figure 10.2.1. But it is interesting to notice that the ratio of the reflectance at 0.6µm and 1.6µm could be efficient to separate low (water) clouds from dust.

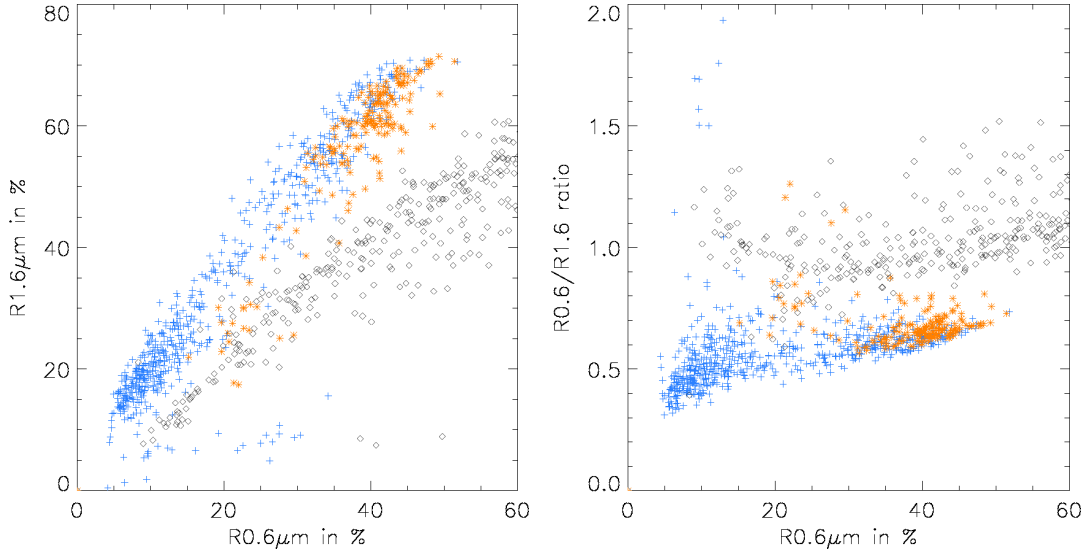

Figure 10.2.1 Left: Variation of R1.6µm reflectance (left) and R0.6µm/ R1.6µm reflectance ratio (left) with R0.6µm reflectance. For continental cloud free surface (blue +), low clouds (black diamond) and dust (brown *)

- At daytime, the presence of dust induces respectively a decrease and increase of T10.8µm-T12.0µm and T8.7µm-T10.8µm brightness temperature differences of continental surfaces, as shown on figure 10.2.2. We can note that this behaviour is in apparent contradiction with simulations presented in Ackerman, 1997. These features are not straightforward to use (as it was the case over sea), because of the large natural variability of the these quantities over land (illustrated on figure 10.2.2) which is difficult to

accurately simulate. Additionally, the T10.8µm-T12.0µm allows an easy distinction from clouds.

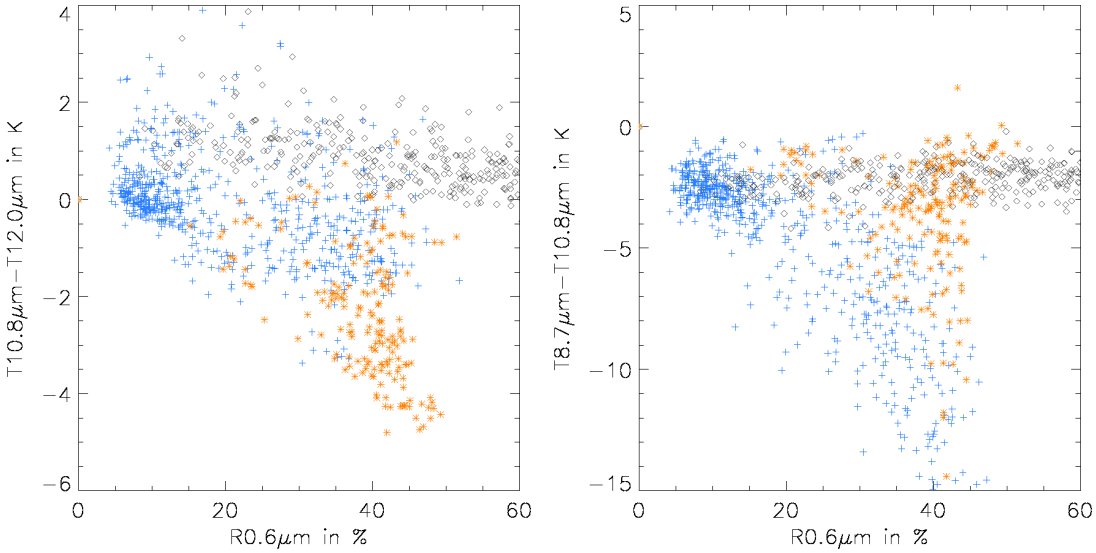

Figure 10.2.2 Variation of T10.8µm-T12.0µm and T8.7µm-T10.8µm brightness temperature differences with R0.6µm reflectance. For continental cloud free surface (blue +), low clouds (black diamond) and dust (brown *)

- When prototyping SAFNWC algorithms with AVHRR and GOES (see Ref [1]), T3.9µm-T10.8µm was found very useful to identify dust at daytime using AVHRR imagery (see figure 10.2.3 (right)). In fact dust was characterised by large T3.9µm-T10.8µm values, as simulated in Ackerman, 1989. But the impact of dust on this brightness temperature difference seems lower in MODIS imagery than in AVHRR (NOAA-14) (see figure 10.2.3). One explanation is a smaller thermal contrast between dust and surface with MODIS (on board EOS-TERRA morning satellite) than with AVHRR (on board NOAA-14 afternoon satellite). It could also be due to stronger atmospheric absorption in MODIS channel (see figure 8.1.3). Nevertheless, this feature seems more efficient than T10.8µm-T12.0µm and T8.7µm-T10.8µm.

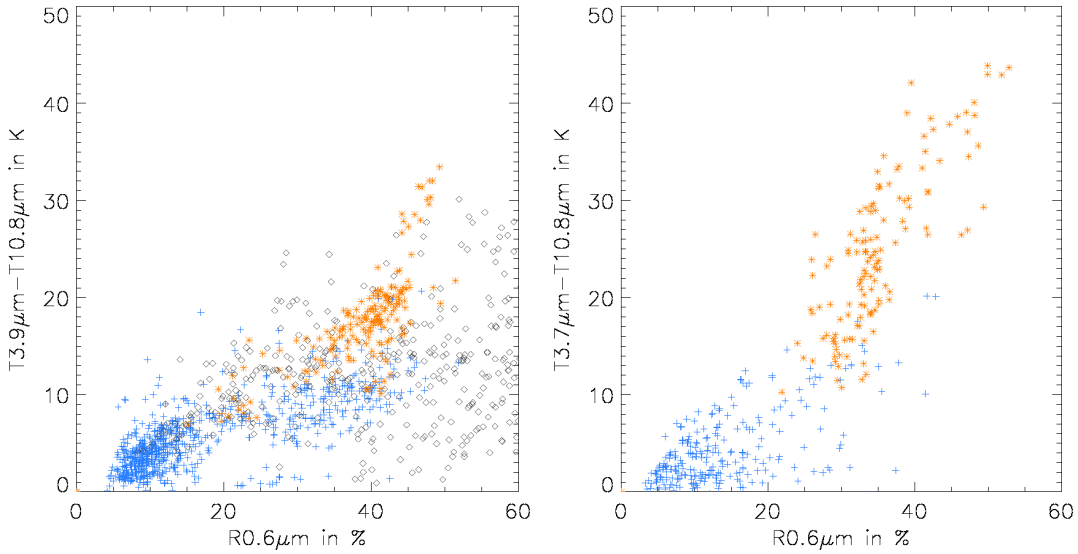

Figure 10.2.3 Variation of T3.9µm-T10.8µm (T3.7µm-T10.8µm for AVHRR) brightness temperature difference with visible reflectance for MODIS targets (left) and AVHRR targets (right). Continental cloud free surface (blue +), dust (brown *) and low clouds (black diamond).

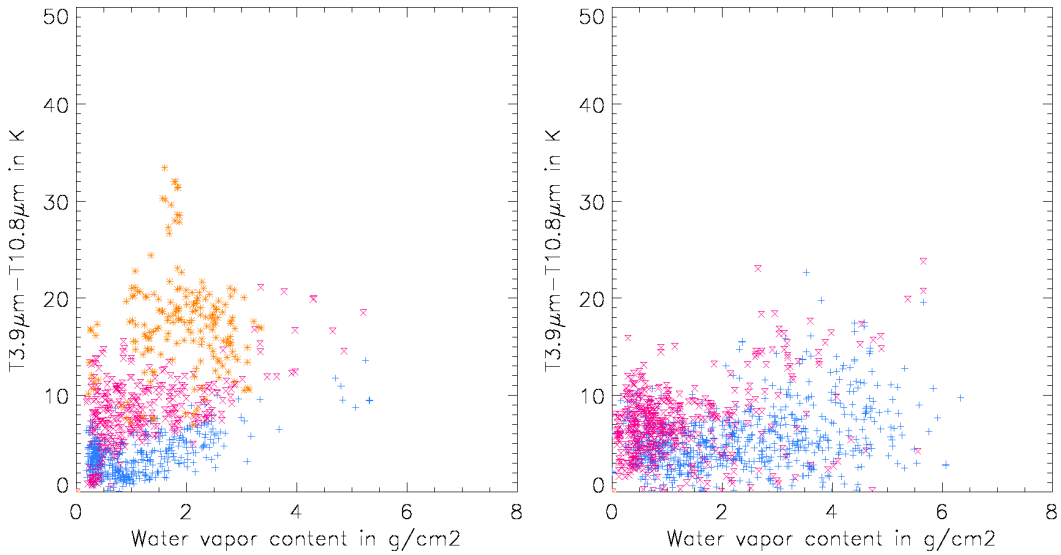

Figure 10.2.4 Variation of daytime T3.9µm-T0.8.0µm brightness temperature difference with water vapour. Left: for MODIS targets. Right: GOES targets
Dark continental cloud free surface(visible reflectance lower than less than 15%): blue +,
Bright continental cloud free surface(visible reflectance larger than less than 15%): purple,
Dust (brown *).

As a conclusion, the 1.6µm channel will not be used to improve the dust identification over continental areas. Instead, T8.7µm-T10.8µm and T10.8µm-T12.0µm will be included in an updated algorithm that will be tested before being implemented in the SEVIRI scheme:

Over the land at daytime, a pixel is classified as contaminated by dust if:

- R06threshold –15% < R0.6µm < R06threshold + 30%
- 0°C < T10.8µm < 37°C
- T3.9µm -T10.8µm > threshold [TBD: constant values (around 15 °C) or f_1(R0.6µm)]
- T10.8µm -T12.0µm < threshold [TBD: constant values (around 0°C) or f_2(R0.6µm)]
- T8.7µm -T10.8µm > threshold [TBD: T87T108threshold or f_3(R0.6µm)]
- SD(10.8µm) < 0.4°C and SD(0.6µm) < 0.6%

[R06threshold and T87T108threshold are the threshold used in the cloud detection process, SD is the standard deviation,].

No scheme can be yet proposed for nighttime or twilight conditions, as even a visual identification of dust is difficult.

REFERENCES

[1] SAFNWC scientific documentation: Prototype Scientific Description for Meteo-France/CMS. Fevrier 2000.

[2] User manual for the PGE01-02-03 of the SAFNWC / MSG : Scientific part. June 2001

[3] Ackerman S.A, 1989, Using the radiative temperature difference at 3.7 and 11mm to track dust outbreaks, *Remote Sensing of Environment*, **27**, 129-133

[4] Ackerman S.A., 1997, Remote sensing aerosols using satellite infrared observations, *Journal of geophysical research*, **102(D14),**17069-17079

[5] Chevalier F., 1999, TIGR-like sampled databases of atmospheric profiles from the ECMWF 50-level forecast model. NWPSAF Research report n°1

[6] Salisbury J.W., D'Aria D.M., Wald A., 1994, Measurements of thermal infrared spectral reflectance of frost, snow and ice, *Journal of geophysical research*, **99(B12),**24235-24240

[7] Strabala K., Ackerman S., 1994, Cloud properties inferred from the 8-12µm data, *Journal of Applied Meteorology*,**33**,212-229.

[8] Thompson G., Lee T.F., Vivekanandan J., 1997, Comparisons of satellite-based aircraft icing diagnoses. *7th Conf.on Aviation, Range and Aerospace Meteorology, 2-7 February 1997.*

[9] Watts P., 1996, Estimation of cloud droplet size, optical depth and phase from the Along Track Scanning Radiometer, *IRS'96 Current Problems in Atmospheric Radiations*.

[10] Hillger D., 1999, Using the new 1.6µm channel on NOAA-15 in satellite product development. *10th Conference on Atmospheric Radiation (28June-2 July 1999)*, pp193-196.

ACRONYMS

AVHRR	Advanced Very High Resolution Radiometer
CMa	Cloud Mask (also called PGE01)
CT	Cloud Type (also called PGE02)
EOS	Earth Observing System
GOES	Geostationary Operational Environmental Satellite
MODIS	Moderate-Resolution Imaging Spectroradiometer
MSG	Meteosat Second Generation
PGE	Product Generation Element
R0.6µm	0.6 visible reflectance
SAFNWC	SAF to support NoWCasting and very short range forecasting
SEVIRI	Spinning Enhanced Visible & Infrared Imager
SST	Sea Surface Temperature
T10.8µm	10.8 micrometer infrared brightness temperature